


Article

Downregulation of miR-192 Alleviates Oxidative Stress-Induced Porcine Granulosa Cell Injury by Directly Targeting Acvr2a

Jiaqing Zhang¹, Qiaoling Ren¹, Junfeng Chen¹, Lingyan Lv², Jing Wang¹, Ming Shen³ , Baosong Xing^{1,*} and Xianwei Wang^{4,*}

¹ Henan Key Laboratory of Farm Animal Breeding and Nutritional Regulation, Institute of Animal Husbandry and Veterinary Science, Henan Academy of Agricultural Sciences, Zhengzhou 450002, China; zhangjq@hnagri.org.cn (J.Z.); renql@163.com (Q.R.); afeng008@163.com (J.C.); wangjing@hnagri.org.cn (J.W.)

² Animal Husbandry Research Institute of Guangxi, Nanning 530001, China; llyan159@163.com

³ College of Animal Science and Technology, Nanjing Agricultural University, Nanjing 210095, China; shenm2015@njau.edu.cn

⁴ Henan Provincial Animal Husbandry General Station, Zhengzhou 450008, China

* Correspondence: xingbaosong502@163.com (B.X.); wangxianwei2008@163.com (X.W.)

Abstract: Follicular atresia is primarily caused by breakdown to granulosa cells (GCs) due to oxidative stress (OS). MicroRNAs (miRNAs) elicit a defense response against environmental stresses, such as OS, by acting as gene-expression regulators. However, the association between miRNA expression and OS in porcine GCs (PGCs) is unclear. Here, we examined the impact of H₂O₂-mediated OS in PGCs through miRNA-Seq. We identified 22 (14 upregulated and 8 downregulated) and 33 (19 upregulated and 14 downregulated) differentially expressed miRNAs (DEmiRNAs) at 100 μM and 300 μM H₂O₂, respectively, compared with the control group. Among the DEmiRNAs, mi-192 was most induced by H₂O₂-mediated OS, and the downregulation of miR-192 alleviated PGC oxidative injury. The dual-luciferase reporter assay results revealed that miR-192 directly targeted Acvr2a. The Acvr2a level was found to be remarkably decreased after OS. Furthermore, grape seed procyanidin B2 (GSPB2) treatment significantly reduced the H₂O₂-induced upregulation of miR-192, and decreased PGC apoptosis and oxidative damage. Meanwhile, GSPB2 prevented an H₂O₂-induced increase in caspase-3 activity, which was enhanced by the application of the miR-192 inhibitor. These results indicate that GSPB2 protects against PGC oxidative injury via the downregulation of miR-192, the upregulation of Acvr2a expression, and the suppression of the caspase-3 apoptotic signaling pathway.

Keywords: oxidative stress; granulosa cell apoptosis; miRNA; GSPB2



Citation: Zhang, J.; Ren, Q.; Chen, J.; Lv, L.; Wang, J.; Shen, M.; Xing, B.; Wang, X. Downregulation of miR-192 Alleviates Oxidative Stress-Induced Porcine Granulosa Cell Injury by Directly Targeting Acvr2a. *Cells* **2022**, *11*, 2362. <https://doi.org/10.3390/cells11152362>

Academic Editor: Artur Mayerhofer

Received: 2 July 2022

Accepted: 26 July 2022

Published: 1 August 2022

Publisher's Note: MDPI stays neutral with regard to jurisdictional claims in published maps and institutional affiliations.



Copyright: © 2022 by the authors. Licensee MDPI, Basel, Switzerland. This article is an open access article distributed under the terms and conditions of the Creative Commons Attribution (CC BY) license (<https://creativecommons.org/licenses/by/4.0/>).

1. Introduction

The ovarian follicles constitute oocytes, which are structurally connected to specialized somatic cells called granulosa cells (GCs) [1]. The GCs facilitate the growth of ovarian follicles by supporting the development of oocytes, and the production of sex steroids and other growth factors. GC dysfunction has been associated with several ovarian malfunctions, including polycystic ovarian syndrome (PCOS), premature ovarian insufficiency (POI), and premature ovarian failure (POF) [2]. Under aerobic conditions, GCs experience an oxygen paradox. GCs require oxygen to maintain their function [3]. In ovarian follicles, low levels of reactive oxygen species (ROSs), such as superoxide ion (O²⁻), singlet oxygen (1O₂), hydroxyl radical (OH·), ozone (O₃), hydrogen peroxide (H₂O₂), etc., facilitate GC signaling and homeostasis [4]. However, environmental stress and other pathological conditions can promote a dramatic enhancement in the ROS levels, resulting in severe cellular dysfunction, such as enzyme inactivation, mitochondrial abnormalities, and DNA fragmentation [5,6]. Thus, an overproduction of ROSs and/or a deficiency in antioxidants cause an imbalance

in ROS-related regulatory mechanisms, resulting in oxidative stress (OS) in ovarian follicles [7]. Previous studies have shown a link between OS and ovarian toxicity in a rodent model exposed to diverse stimuli, such as gamma irradiation, chemotherapeutic drugs, or polycyclic aromatic hydrocarbons [8,9]. Additionally, ROSs derived from oxidants, such as methoxychlor, nicotine, H₂O₂, D-galactose, and 3-nitropropionic acid, have been found to induce mouse GC apoptosis in antral follicles [8,10].

Previous studies have shown that OS may lead to decreased reproductive efficiency of sows and delayed puberty in gilts. Reproductive disorders, including abnormal embryonic development, anovulation, etc., cause the culling of approximately half of the total number of sows culled annually. On commercial farms, there are many stressful stimuli, such as pregnancy, lactation, weaning, and high stocking density, which induce a rapid increase in ROS levels and cause OS in the maternal body. Furthermore, OS is known to promote reproductive disorders in replacement gilts and highly prolific sows [11,12]. OS plays a role in pathological progression by influencing multiple physiological processes from follicle development to oocyte maturation. Previous studies have indicated that high levels of ROS regulate the expression of epigenetic and transcriptional factors [6,10].

MicroRNAs (miRNAs) are small, noncoding RNAs (approximately 19 to 24 nucleotides) that function as gene-expression regulators and modulate cellular differentiation, proliferation, and apoptosis [13]. Recently, the aberrant expression of miRNAs has been corroborated in GC pathophysiology and ovarian endocrine abnormalities [14]. Our previous studies have shown that oxidant (H₂O₂, 3-NP, and diquat)-induced elevation in ROS levels promote cytotoxicity and cell death in GCs [5,9]. Additionally, recent studies have demonstrated that specific miRNAs are involved in OS-induced GC apoptosis [6,15]. However, the regulation of miRNA expression by OS in porcine GC (PGC) is unclear. In the present study, H₂O₂ was used to stimulate porcine GCs (PCGs) as an OS cell model, and the potential interaction of differentially expressed miRNAs (DEmiRNAs) with targeted mRNAs in H₂O₂-induced PGCs was analyzed using bioinformatics methods. The results will enhance our understanding of the potential biological relevance of miRNAs in PGCs exposed to OS.

2. Materials and Methods

2.1. Animals

Ovarian samples were obtained as described previously [1]. Animal procedures were performed in compliance with the guidelines of the Institutional Animal Care and Use Committee of Animal Husbandry and Veterinary Science, Henan Academy of Agricultural Sciences. The approval number for this study is IACUC-20190820002.

2.2. Cell Culture and Reagents

GCs, collected from healthy follicles (diameter: 3–5 mm), were cultured at 37 °C in T25 flasks containing DMEM/F-12 medium (Gibco, Grand Island, NY, USA) 10% FBS, and 1% penicillin-streptomycin (Gibco, Grand Island, NY, USA) in 5% CO₂. For drug administration, GCs were treated with 0 to 1000 μM H₂O₂ for 12 h. The following miRNAs were transfected GCs: miR-192 mimics, miR-192 inhibitor, negative control (NC) mimics, and inhibitor NC (Shanghai Gene Pharma, Shanghai, China); this was achieved using Lipofectamine reagent (Invitrogen, Shanghai, China) according to the manufacturer's protocol.

2.3. GC Viability Assay

A Cell Counting Kit 8 assay (CCK-8; DOJINDO Laboratories, Japan) was used to measure GC viability following the protocol. GCs were cultured in 96-well plates until they were 90% confluent (5×10^4 cells/well), followed by treatment with 0 to 500 μM H₂O₂ for 12 h. Post-treatment, in each well, the CCK-8 solution (10 μL) and 100 μL medium were incubated for 2 h at 37 °C. A microplate reader was used to estimate GC viability at 450 nm (Bio-Rad, Hercules, CA, USA).

2.4. Detection of Intracellular ROS

ROS levels in porcine GCs were measured using the GENMED intracellular-ROS red-fluorescence determination kit (GENMED, GMS10111.1; Shanghai, China). The detailed procedure was performed according to the manufacturer's instructions. ROS levels in porcine cells were determined by measuring the oxidative conversion of dihydroethidium bromide into ethidium bromide, which emits red fluorescence when bound to DNA in the nuclei. Images were taken using an Olympus IX-73 fluorescence microscope (Olympus, Tokyo, Japan). The fluorescence intensity was evaluated in each GC using ImageJ 1.42q software (NIH).

2.5. Apoptosis Analysis

The TUNEL kit (Roche Applied Science, Penzberg, Germany) was used for analyzing GC apoptosis following the manufacturer's guidelines. The Olympus IX-73 fluorescence microscope was used to capture images. A total of five fields of vision were selected to count the numbers of apoptosis cells and total cells. Then, the rate of apoptosis of PGCs was calculated. All experiments were repeated at least 3 times.

2.6. Caspase-3 Activity Assay

Caspase-3 activity was examined using caspase-3 activity assay kits (Beyotime Institute of Biotechnology) according to the manufacturer's instructions. Briefly, the GCs were homogenized in 10 mL reaction buffer containing 1 mL Caspase-3 fluorogenic substrate Ac-DEVD-pNA (acetylAsp-Glu-Val-Asp p-nitroanilide) and incubated for 2 h at 37 °C. Cleavage of the substrates was measured at 405 nm using a microplate reader.

2.7. Small-RNA Library Construction and Sequencing

The TRIzol reagent was used to isolate total RNA following the specified protocol. The Bioanalyzer 2100 (Agilent, Santa Clara, CA, USA) with a RIN > 7.0 was used for analyzing the purity and quantity of the extracted RNA. A small-RNA library was built using the TruSeq Small-RNA Sample Prep Kit (Illumina, San Diego, CA, USA) using total RNA (1 µg). Then, the Illumina HiSeq 2500 was used to perform single-end sequencing (36 bp or 50 bp) at LC-BIO (Hangzhou, China).

2.8. Data Analysis

The raw reads were subjected to ACGT101-miR (LC Sciences, Houston, TX, USA), an in-house program, to remove junk, adapter dimers, common RNA families (rRNA, tRNA, snRNA, and snoRNA), low complexity, and repeats. Next, we used BLAST to map unique 18- to 26-nucleotide-long sequences to specific precursors in miRBase 21.0 to detect the known miRNAs (in the hairpin arms) and novel 3p-derived and 5p-derived miRNAs (in the arm opposite the annotated mature miRNA-containing arm). The alignment parameters allowed length variations at both the 5' and 3' ends, as well as one sequence mismatch. The known miRNAs were classified as the unique sequences that mapped mature miRNAs in hairpin arms to specific species. Next, we used BLAST to map the remaining sequences to other species precursors, except for certain species, in the miRBase 21.0; this was followed by estimation of their genomic location by mapping the pre-miRNAs against the specific species genomes using BLAST. These two categories were classified as the known miRNAs. Next, using BLAST software, we aligned the unmapped sequences against the specific genomes and used the RNAfold software to predict the hairpin RNA structures containing sequences from the flank 80 nt sequences. The secondary structure was predicted based on the following criteria: (1) less than or equal to 12 nucleotides in one bulge in the stem; (2) cutoff of free energy ($\text{kCal/mol} \leq -15$); (3) length of the hairpin loop (≤ 20); (4) less than or equal to 4 biased errors in one bulge in the mature region; (5) less than or equal to 7 errors in mature region; (6) greater than or equal to 80% maturity in the stem; (7) more than 16 base pairs in the stem region of the predicted hairpin; (8) length of the hairpin (up and down stems + terminal loop ≥ 50); (9) less than or equal to 8 nucleotides in one bulge

in the mature region; (10) less than or equal to 2 biased bulges in the mature region; (11) more than or equal to 12 base pairs in the mature region of the predicted hairpin. All data have been deposited into the NCBI Gene Expression Omnibus and are accessible via GEO series accession number GSE201369.

2.9. Analysis of Differentially Expressed miRNAs

A χ^2 -squared 2×2 test, a Student's *t*-test, an ANOVA, a Fisher's exact test, or an $n \times n$ test were used to examine the differential expression of miRNAs based on normalized deep-sequencing counts. For each test, the limit of statistical significance was set between 0.01 and 0.05.

2.10. The Prediction of Target Genes of miRNAs

We used miRanda 3.3a and TargetScan 50 to identify the miRNA binding sites to estimate the target genes of DE miRNAs. We combined the prediction data from both algorithms to obtain the overlapping results. We also annotated the GO terms and KEGG pathways of the targets of these DE miRNA.

2.11. Quantitative Real-Time RT-PCR (qRT-PCR)

Total RNA was extracted from PGCs using the TRIzol reagent according to the manufacturer's protocol. Firstly, total RNA was reverse-transcribed using the M-MLV reverse transcriptase (Takara, Dalian, China). Then, qRT-PCR reactions were performed using a standard SYBR Green PCR kit. The 20 μ L reaction mixture contained 10 μ L of $2 \times$ SYBR Premix Ex Taq, 1 μ L 10 μ M of each primer, 2 μ L of cDNA, and 7 μ L of ddH₂O. qRT-PCR for each gene was performed in triplicate for each sample using a Roche Light Cycler 480 system with SYBR Green Real-Time PCR Mix (Takara, Dalian, China). The mRNA primers for Bim, Bax, and Acvr2a were based on those used in previously published studies [16–18]. GAPDH was used as an internal control. The miRNA was extracted from the control and the H₂O₂ treatment samples (100 and 300 μ M) using a miRNA extraction kit (Tiangen Biotech, Beijing, China). First, the miRcute Plus miRNA First-Strand cDNA Synthesis Kit was used to synthesize cDNA. The reaction mix (20 μ L), consisting of total RNA (3 μ L), $2 \times$ miRNA RT Reaction Buffer (10 μ L), miRNA RT Enzyme Mix (2 μ L), and ddH₂O (5 μ L), was incubated for 1 h at 42 °C, followed by 3 min at 95 °C for enzyme inactivation. The miRcute Plus miRNA qPCR Detection Kit (SYBR Green) (Tiangen Biotech, Beijing, China) was used to quantify miRNA. Primers for miR-181d-5p (cat. no. CD201-T), miR-23b-5p (cat. no. CD201-0311), miR-129-1-3p (cat. no. CD201-0200), miR-19b-3p (cat. no. CD201-0278), miR-190b (cat. no. CD201-T), miR-375-3p (cat. no. CD201-0173), miR-192 (cat. no. CD201-0082), miR-339-5p (cat. no. CD201-T) and U6 (cat. no. CD201-0145) were acquired from Tiangen Biotech Co., Ltd (Beijing, China). The relative miRNA expression levels were derived using the $2^{-\Delta\Delta C_t}$ method [19].

2.12. Western Blot Analysis

Total proteins were prepared using protein lysis buffer and quantified using a BCA protein assay kit (Beyotime, Beijing, China). Next, 20 μ g of total protein/sample was loaded onto a 12% SDS-polyacrylamide gel and transferred onto a PVDF membrane (Millipore, Billerica, MA, USA) via electroblotting. Non-specific binding sites were blocked with 5% bovine serum albumin in TBST for 1.5 h. Then, the membranes were incubated with primary antibodies against ACVR2A (DF6733, Affinity Biosciences, Cincinnati, OH, USA), Cleaved-Caspase 3 (AF7022, Affinity Biosciences, Cincinnati, OH, USA), and GAPDH (BM1623, Boster Biological Technology, Wuhan, China) overnight at 4 °C; all primary antibodies were used at a dilution of 1:200 in PBS containing 5% bovine serum albumin. Immunoreactivity was detected via treatment with an appropriate HRP-conjugated secondary antibody. Protein bands were visualized by exposing the blots to an enhanced chemiluminescence detection system (LAS-4000 imager, Fujifilm, Tokyo, Japan).

2.13. Statistical Analysis

SPSS v17.0 (SPSS, Armonk, NY, USA) was used for data analyses, and the results are represented as the means \pm standard error (S.E.). *p*-values of less than 0.05 and 0.01 were considered significant and extremely significant differences, respectively.

3. Results

3.1. OS Reduces Viability and Induces Apoptosis in PGCs

The primary cultured PGCs were treated with various concentrations of H₂O₂ (0, 50, 100, 200, 300, 500, and 1000 μ M) for 12 h to establish an in vitro OS model. Next, we conducted a CCK-8 assay to examine GC proliferation and viability. H₂O₂ induced a significant time-dependent reduction in cell viability (Figure 1A). At 100 μ M H₂O₂, the experimental group demonstrated considerably lower cell viability than the control group (*p* < 0.05). Furthermore, at higher concentrations of H₂O₂, a substantial reduction in cell viability was observed (*p* < 0.01). Thus, doses of 100 μ M and 300 μ M H₂O₂ were chosen as the preferred doses for subsequent experiments.

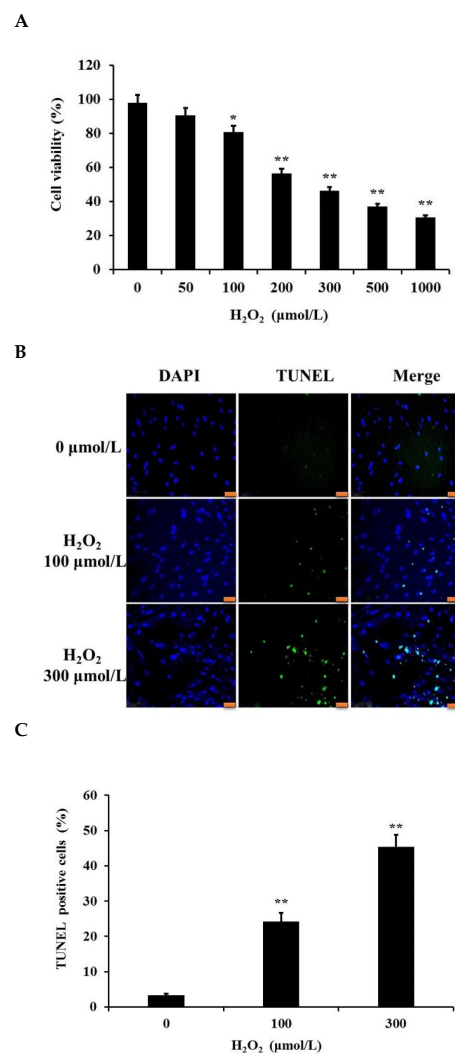


Figure 1. The H₂O₂-mediated OS model in PGCs. (A) Primary cultured GCs were treated with different concentrations of H₂O₂ for 12 h. The CCK-8 assay was used to determine GC viability. (B) GC apoptosis was determined via TUNEL analysis; scale bars correspond to 50 μ m. (C) The average number of TUNEL-positive nuclei/visual fields was used to quantify GC apoptosis. Data represent mean \pm S.E.; each group: *n* = 3. * *p* < 0.05, ** *p* < 0.01 compared to control group.

Next, cultured GCs were treated with 0, 100, and 300 μM H_2O_2 for 12 h, followed by a TUNEL assay to examine the rate of apoptosis. The rate of apoptosis increased with an increase in H_2O_2 concentration (Figure 1B,C). At 100 μM H_2O_2 , a considerable increase in GC apoptosis was observed ($p < 0.05$), which further increased at 300 μM H_2O_2 . These data suggest that H_2O_2 induced dose-dependent apoptosis of PGC, which resulted in reduced cell viability.

3.2. Identification of H_2O_2 -Induced Changes in miRNA Expression in PGCs

We treated PGCs with H_2O_2 to develop a cellular model of OS to understand the impact of H_2O_2 -induced OS on miRNAs. Based on the above results, 100 μM and 300 μM H_2O_2 were chosen as the low concentration (LOS) and the high concentration (MOS) for miRNA profiling, respectively. After treating PGCs for 12 h, the miRNA profiles were analyzed using a high-throughput sequencing strategy. Overall, 22 DE miRNAs (14 upregulated and 8 downregulated) were identified between the LOS group at $|\log_2(\text{foldchange})| \geq 1$ and $p\text{-value} < 0.05$ and the control group (CON) (Figure 2A). Furthermore, 33 DE miRNAs (19 upregulated and 14 downregulated) were identified between the MOS group and the CON group under identical criteria (Figure 2B). Supplementary Table S1 lists all the DE miRNAs. These data indicate that a low concentration of H_2O_2 had a minor effect on the miRNA expression of PGCs, while a high concentration of H_2O_2 could affect the expression of several miRNAs. To validate the accuracy of the sequencing data, eight miRNAs with significantly altered expression were selected for RT-PCR detection. The results agree with the sequencing data, suggesting the high accuracy of our sequencing analysis (Figure 2C).

3.3. Functional Analysis of DE miRNAs

The miRNAs play their functional roles by binding to the complementary site in the 3'-untranslated regions of their target mRNAs. The target genes of H_2O_2 -sensitive miRNAs were analyzed using miRanda and TargetScan. The results revealed that LOS-induced miRNAs targeted 14,244 genes (Supplementary Table S2), and MOS-induced miRNAs targeted 20,568 genes (Supplementary Table S3). Next, we performed KEGG and GO enrichment analyses to detect the cellular functions of these genes in PGCs under OS. The top 20 gene clusters involving biological processes and pathway analyses sensitive to low concentrations of H_2O_2 are summarized in Figure 3A,B. The most significant biological processes included transcriptional regulation, signal transduction, DNA-templated, positive regulation of transcription from the RNA polymerase II promoter, transport, and the oxidation-reduction process. The most significant pathways were the pathways in cancer, HTLV-I infection, Ras, and Rap1, and the endocytosis signaling pathways. The top 20 gene clusters involving biological processes and pathway analyses sensitive to high concentrations of H_2O_2 are summarized in Figure 3C,D. The most significant biological processes were transcriptional regulation, DNA-templating, the positive regulation of transcription from the RNA polymerase II promoter, signal transduction and transport, and the oxidation-reduction process. The most significant pathways were the pathways in cancer, MAPK, Ras, HTLV-I infection, and Rap1 signaling.

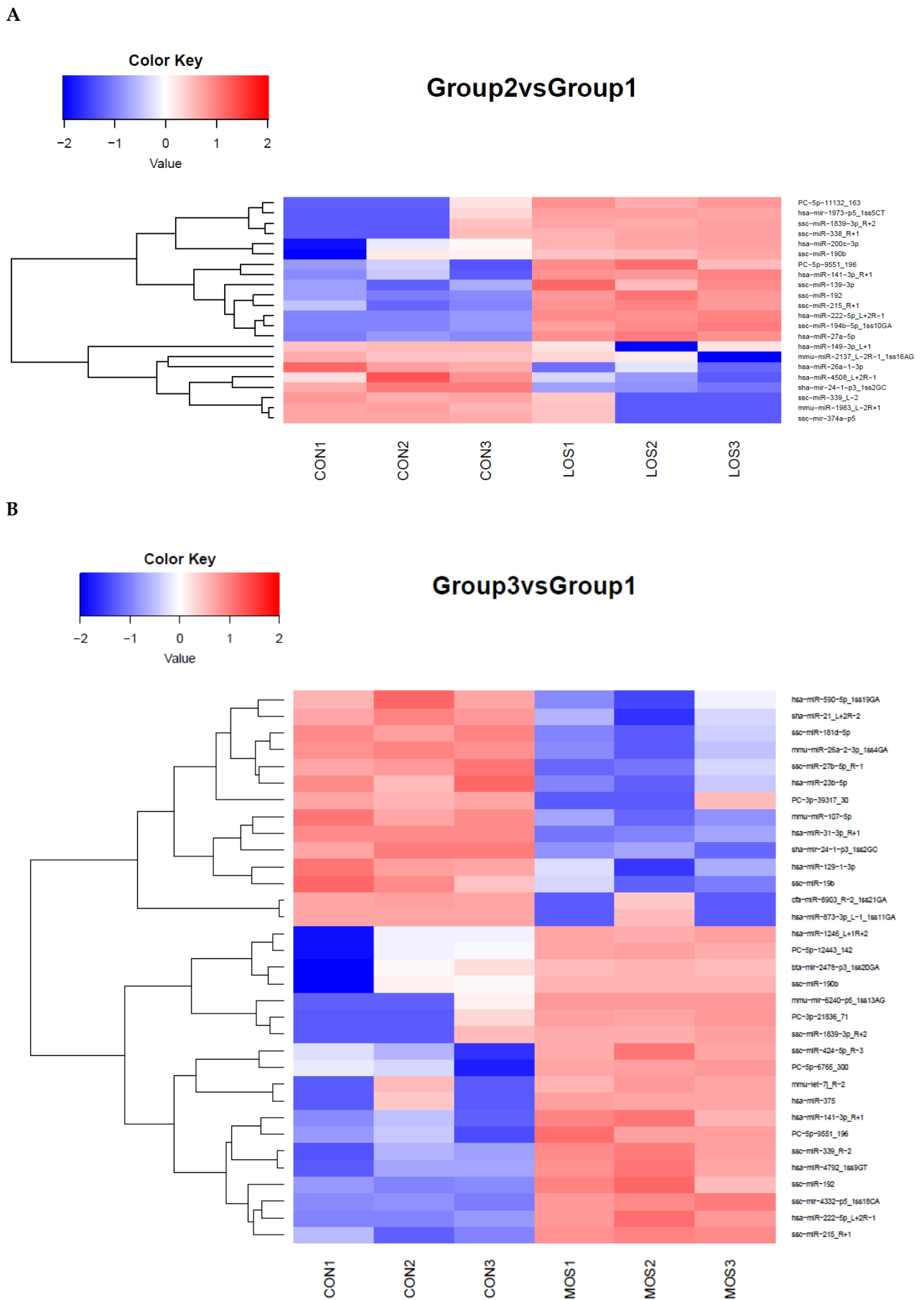


Figure 2. Cont.

C

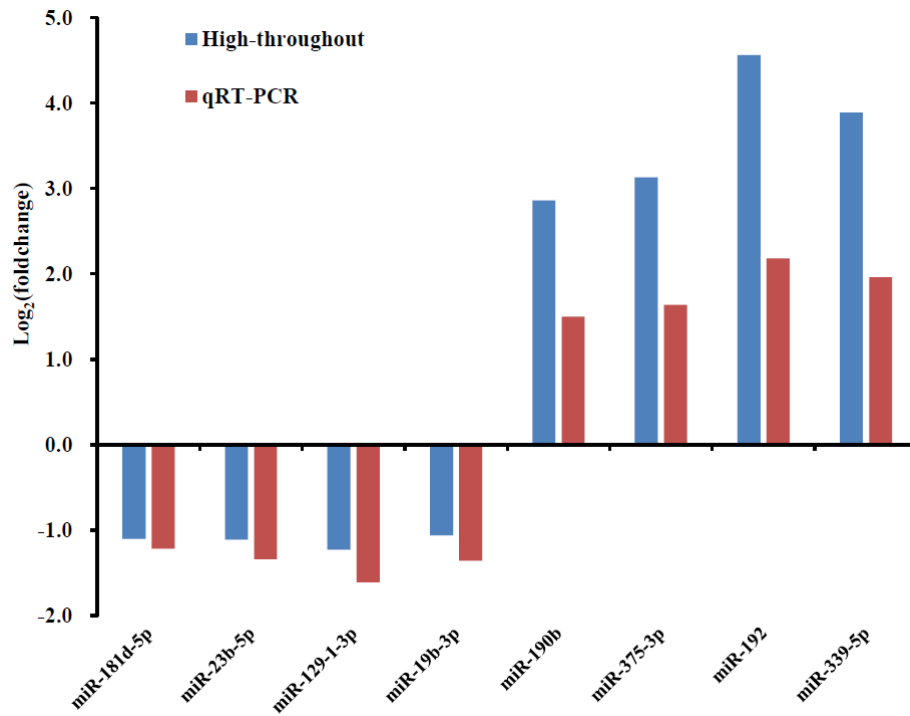
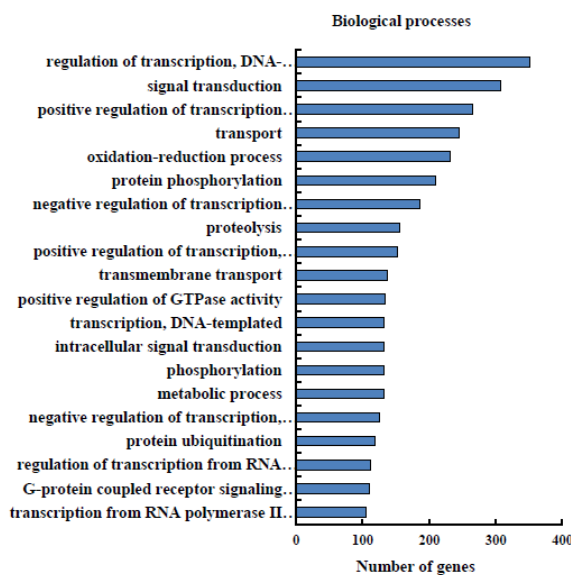


Figure 2. Alterations in the miRNA profiles in H₂O₂ treated PGCs. (A) The heat map of 22 DE miRNAs between low-concentration group (LOS) and normal control (CON). The color scale of the heat map ranges from blue (low expression) to red (high expression). (B) The heat map of 33 DE miRNAs between high-concentration group (MOS) and normal control (CON). Low-concentration group (LOS): 100 μM H₂O₂; high-concentration group (MOS): 300 μM H₂O₂; (C) DE miRNAs with high fold changes were chosen for qRT-PCR validation. Data were normalized using the U6 gene. The data are presented as mean ± S.E. (n = 3). The values are shown as log₂ (fold change).

A



B

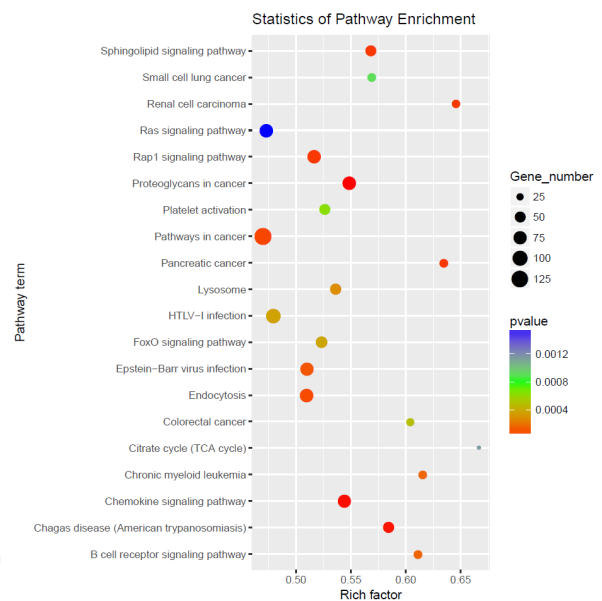


Figure 3. Cont.

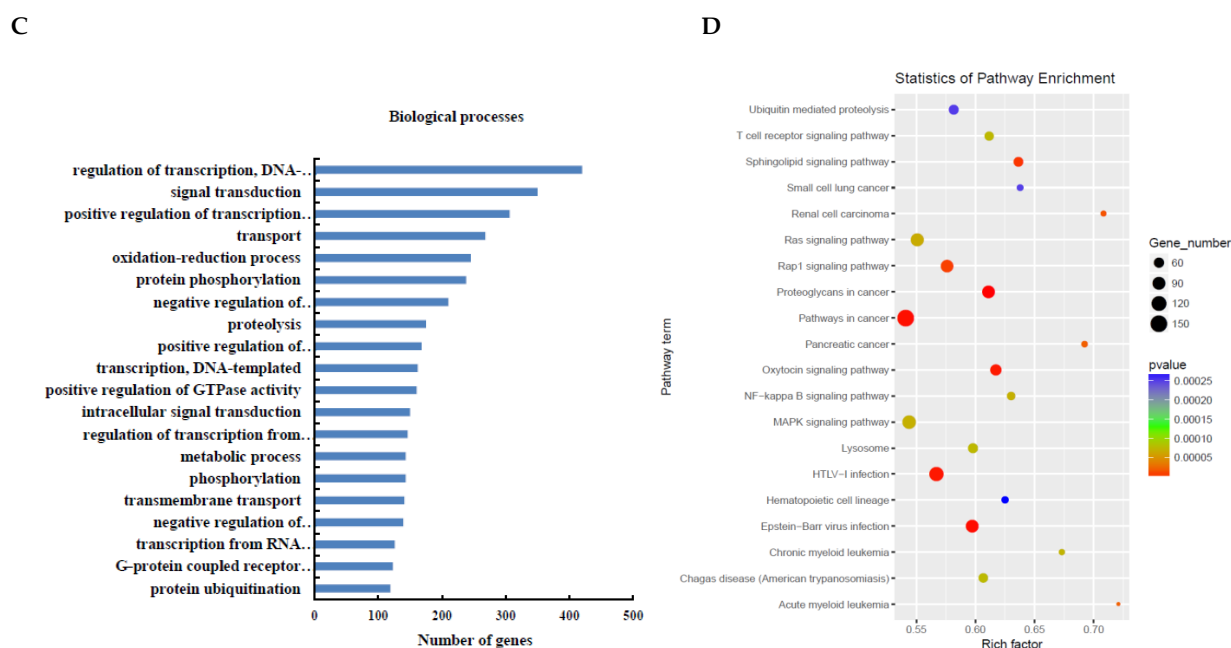


Figure 3. Enrichment analysis of predicted target genes of deregulated miRNAs. (A) Significantly altered cellular processes of predicted target genes of DE miRNAs after H₂O₂ treatment (100 μM). (B) Significantly altered pathways of the target genes. (C) Significantly altered cellular processes of predicted target genes of DE miRNAs after H₂O₂ treatment (300 μM). (D) Significantly altered pathways of the target genes.

Then, we selected overlapping miRNAs between the two concentration groups and further constructed the miRNA-KEGG networks, miRNA-gene networks, and miRNA-GO networks to detect the primary regulatory functions of the overlapping miRNAs and their target genes. We identified 34 pathways by the predicted target genes of 13 DE miRNAs (Figure 4).

Each signaling pathway was co-regulated by more than three miRNAs. The specific miRNAs that co-regulated these pathways are shown in Supplementary Table S4. As shown in Figure 5 and Supplementary Table S5, hsa-miR-141-3p_R+1, PC-5p-9551_196, and hsa-miR-222-5p_L+2R-1, with the target gene numbers 44, 39, and 32, respectively, were the top three miRNAs. Thirteen miRNAs (hsa-miR-141-3p_R+1, PC-5p-9551_196, hsa-miR-222-5p_L+2R-1, hsa-miR-4792_1ss9GT, sha-mir-24-1-p3_1ss2GC, ssc-miR-139-3p, ssc-miR-1839-3p_R+2, ssc-miR-190b, ssc-miR-192, ssc-miR-194a_R+2, ssc-miR-194b-5p_1ss10GA, ssc-miR-215_R+1, and ssc-mir-4332-p5_1ss18CA) were predicted to be involved in apoptosis and autophagy. The top 10 target genes were NR5A1 (nuclear receptor subfamily 5 group A member 1), TGF-β-R1 (transforming growth factor-beta receptor 1), VEGFC (vascular endothelial growth factor C), WNT5A (Wnt family member 5A), RAC1 (Rac family small GTPase 1), MRAS (muscle RAS oncogene homolog), ITGB1 (integrin subunit beta 1), ACVR1B (activin receptor IB), WNT2B (Wnt family member 2B), and SMAD3 (SMAD family member 3).

The DE miRNAs played vital roles in several biological processes, including the activation of MAPK activity (GO:0000187), the apoptotic process (GO:0006915), the cellular response to DNA damage stimulus (GO:0006974), the transforming growth factor-beta receptor signaling pathway (GO:0007179), and the positive regulation of cell population proliferation (GO:0008284) (Figure 6 and Supplementary Table S6). Thus, these results provide us with more comprehensive information on the biological effect of H₂O₂ treatment in PGCs.

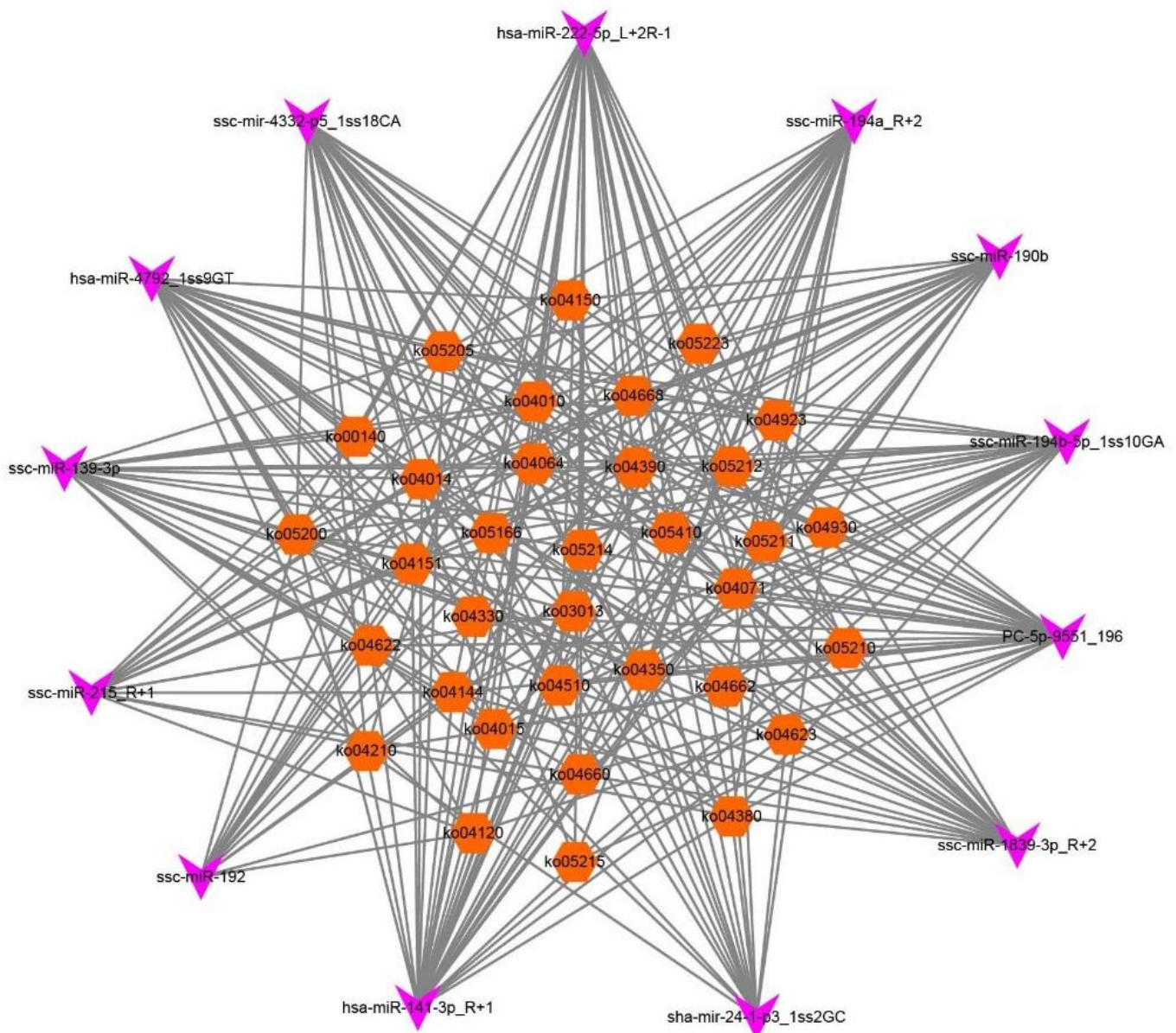


Figure 4. DEMiRNA-KEGG network analysis. The miRNA-KEGG network was built based on the interactions between signal pathways and their respective DEMiRNAs. For the network, the diamond nodes represent miRNA, and the orange nodes represent pathways affected by two/three DE miRNAs.

3.4. miR-192 Overexpression Promotes Porcine GCs Apoptosis

Previous studies showed that miR-192 expression is significantly upregulated in human endothelial cells [20] and animal ovarian tissues [21] under stress. GC apoptosis is the main cause of follicular atresia. Therefore, the role of miR-192 in this process was further studied. The cultured GCs were transfected with miR-192 mimics or mimics NC. Analysis of cell viability showed that the GC proliferation rate was decreased significantly after transfection with the miR-192 mimics ($p < 0.05$; Figure 7A). Furthermore, the number of GC apoptosis was increased significantly after transfection with the miR-192 mimics when compared to those transfected with the mimics NC ($p < 0.05$; Figure 7B,C). It was recently reported that Bim, a BH3-only member of the BCL-2 family, can induce apoptosis by inactivating anti-apoptotic BCL-2 family members and by promoting Bax activation, which subsequently activates caspase-3-mediated apoptosis [22]. As expected, the mRNA expression levels of the apoptotic-related genes (Bax and Bim) were significantly higher in

the GCs transfected with the miR-192 mimics than in those transfected with the mimic NCs ($p < 0.05$; Figure 7D,E). The activity assay suggested that the transfection of miR-192 mimics caused a significant increase in GCs compared with mimics NC ($p < 0.05$; Figure 7F). These results indicate that miR-192 overexpression strongly promoted PGC apoptosis.

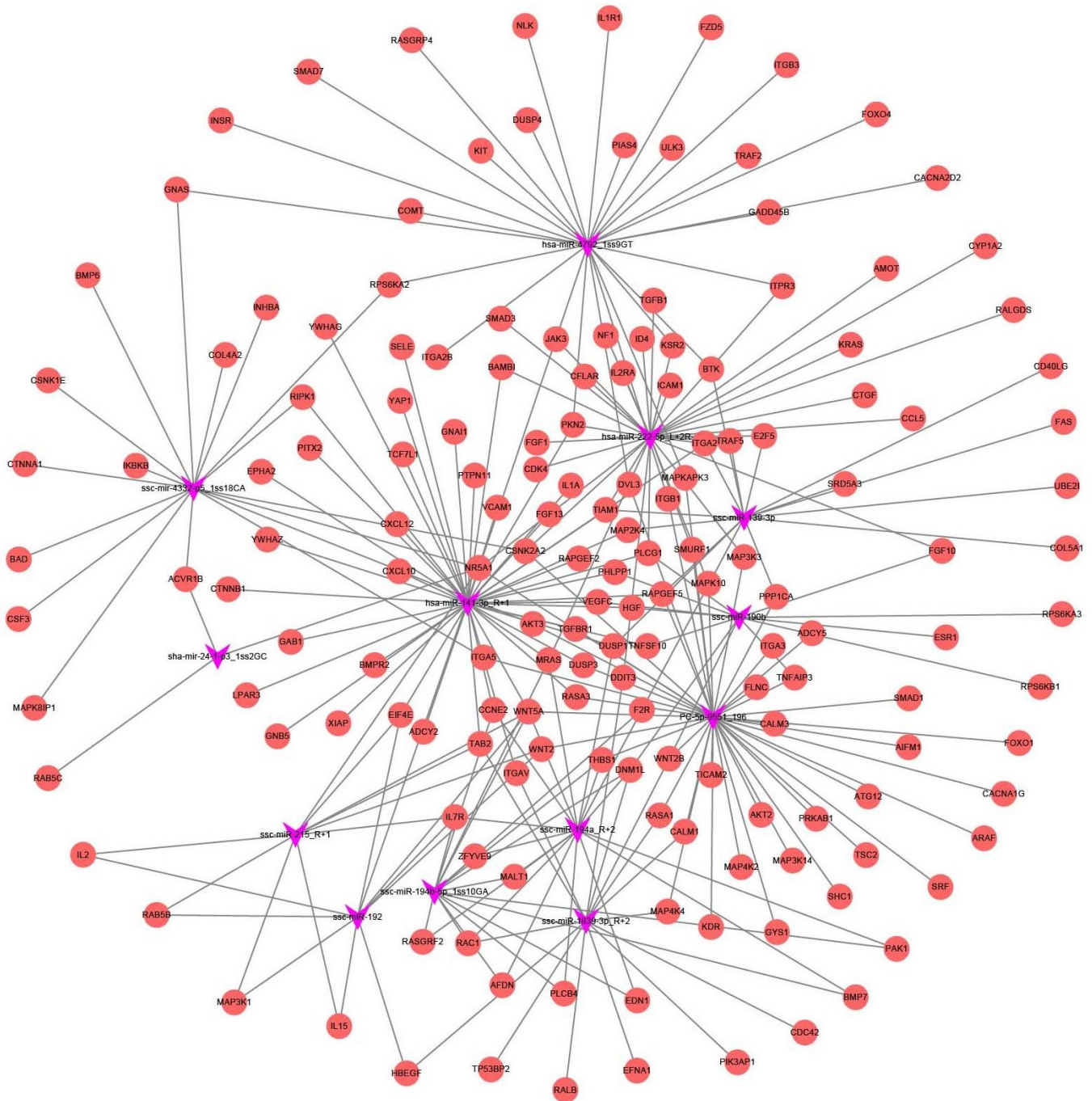


Figure 5. DEMiRNA–Gene network analysis. The miRNA–Gene network was built based on the interactions between miRNAs and the intersected target genes. This analysis illustrates the key regulatory functions of the identified miRNAs and their target genes. For the network, the diamond nodes represent miRNA, and the orange circles represent genes.

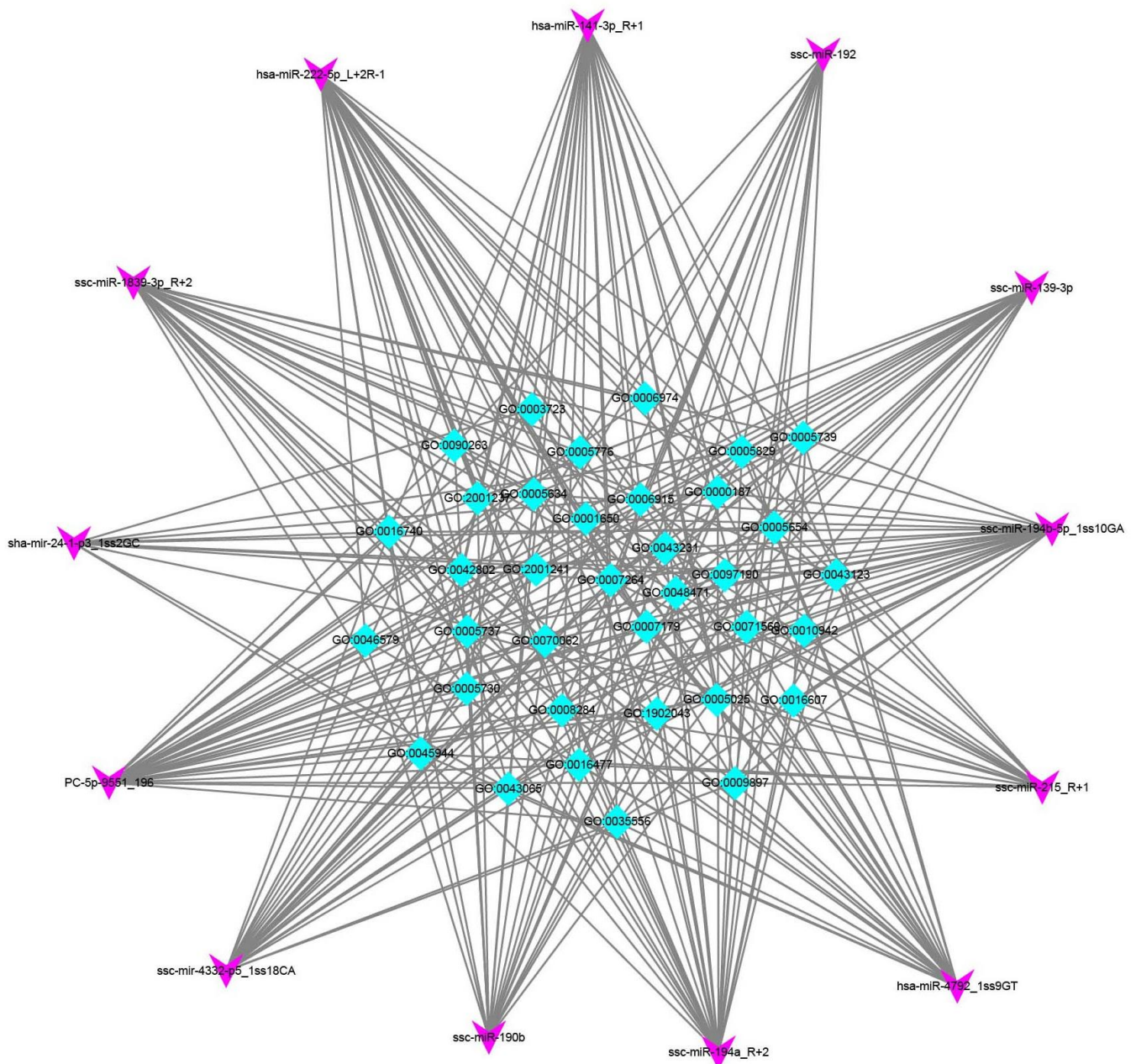


Figure 6. DE miRNA–GO network analysis. The miRNA–GO network was built based on the relationship between significant biological functions and DE miRNAs. The squares represent GOs affected by miRNAs, and the diamond nodes represent miRNA.

3.5. miR-192 Knockdown Counteracts H₂O₂-Induced PGC Injury

Recent studies have demonstrated that miR-192 is involved in the regulation of apoptotic signaling [20]. To further validate whether H₂O₂-induced damage affects the expression of endogenous miR-192 in GCs, the GCs were treated with various concentrations of H₂O₂ (0, 50, 100, 250, and 500 μ M) for 12 h. The expression level of miR-192 was increased significantly by H₂O₂ in a dose-dependent manner (Figure 8A). To assess the effects of miR-192 knockdown on miR-192 expression, cell viability, intracellular ROS levels, and caspase-3 activity, the cultured primary cells were investigated *in vitro*. The expression levels of miR-192 were significantly decreased in the miR-192 inhibitor group compared with the inhibitor control group, and H₂O₂ exposure significantly increased miR-192 expression in the inhibitor control group compared with the expression levels in the miR-192 inhibitor group ($p < 0.05$; Figure 8B). Furthermore, miR-192 knockdown partially rescued

H₂O₂-induced GC viability loss, when compared with the H₂O₂-treated group ($p < 0.05$; Figure 8C). In addition, the cultured GCs transfected with miR-192 inhibitor and treated with H₂O₂ appeared to be less susceptible to H₂O₂-induced injury, as indicated by the lower caspase-3 activity and intracellular ROS levels compared with the H₂O₂-treated inhibitor control group ($p < 0.05$; Figure 8D–F). These results suggest that miR-192 knockdown in porcine GCs may exert a protective effect against H₂O₂-induced injury.

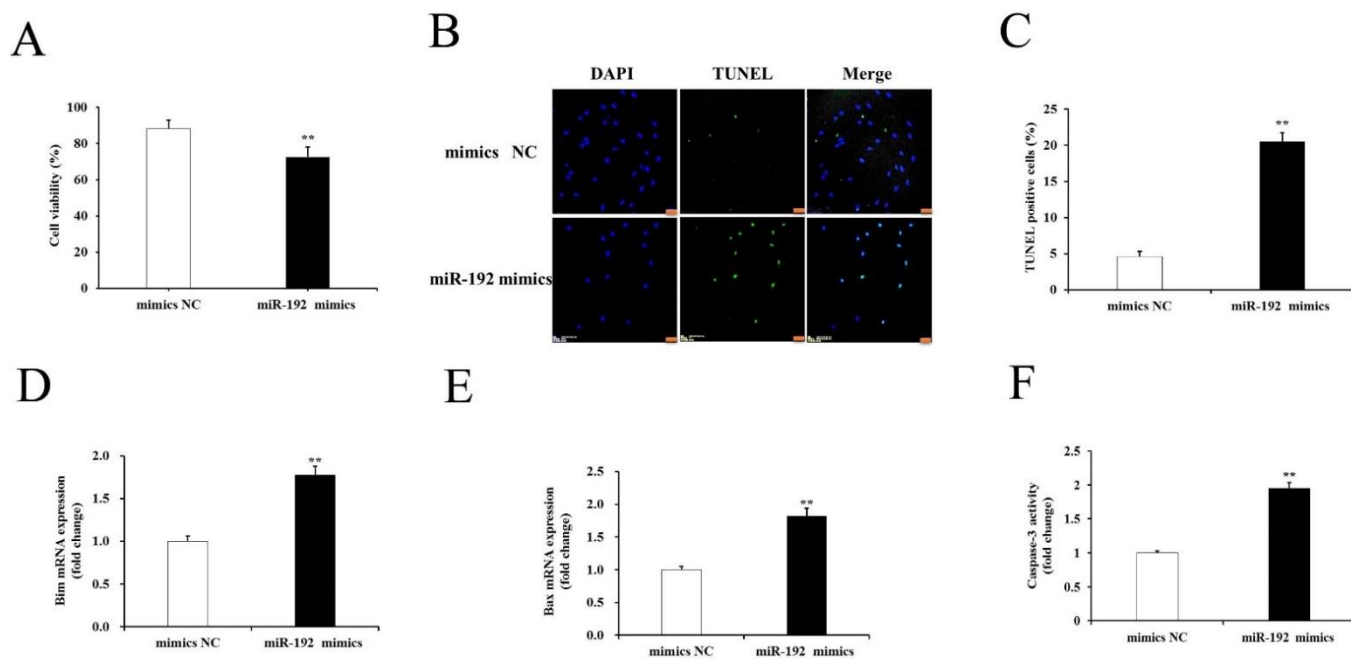


Figure 7. Overexpression of miR-192 induces PGCs apoptosis. (A) Effects of miR-192 overexpression on the proliferation of PGCs. (B) Apoptosis of GCs was evaluated using TUNEL assay; scale bars correspond to 50 μ m. (C) Quantification of TUNEL-positive cells in porcine GCs. (D) The expression analysis of Bim. The relative expression data were normalized to β -actin. (E) The expression analysis of Bax. (F) The analysis of caspase-3 activity. The t -test was used to examine the differences between the groups. Data are presented as the means \pm SE. ($n = 3$). ** $p < 0.01$.

3.6. *Acvr2a* Is a miR-192 Target

Among DEMiRNAs, we found that miR-192 was the most significantly upregulated miRNA in PGCs after qRT-CR validation. Pathway analysis showed that the miR-192 targets are enriched in steroid biosynthesis, the insulin signaling pathway, and the GnRH signaling pathways (Figure 9A). Gene ontology analysis indicated that the miR-192 targets were mainly involved in the regulation of the digestive-system process, the rRNA catabolic process, and RNA surveillance (Figure 9B). *Acvr2a* was identified as a putative miR-192 target; this gene is widely expressed in ovarian GCs, and it is closely related to GC proliferation and follicular development. Therefore, *Acvr2a* was chosen as a candidate target gene for further study. Bioinformatics analysis identified a putative miR-192 binding site in the 3'UTR of *Acvr2a* (Figure 9C). To confirm that *Acvr2a* is a direct target of miR-192, the WT and mutant vectors were co-transfected HEK293T cells with either miR-192 mimics or mimics NC, and their luciferase activity was measured. The results showed that the miR-192 mimic, but not the mimics NC, markedly suppressed the luciferase activity of the *Acvr2a* 3'UTR-WT but not that of *Acvr2a* 3'UTR-MT, suggesting that miR-192 directly targets the 3'-UTR of *Acvr2a* (Figure 9D). To validate that the *Acvr2a* is a target of miR-192, the mRNA and protein expression levels of *Acvr2a* were determined after the transfection of the GCs with the miR-192 mimics or mimics NC. The results indicate that the expression levels of *Acvr2a* mRNA and the ACVR2A protein markedly decreased in GCs transfected

with the miR-192 mimics ($p < 0.05$; Figure 9E,F). These data suggest that *Acvr2a* is a validated target of miR-192 in PGCs.

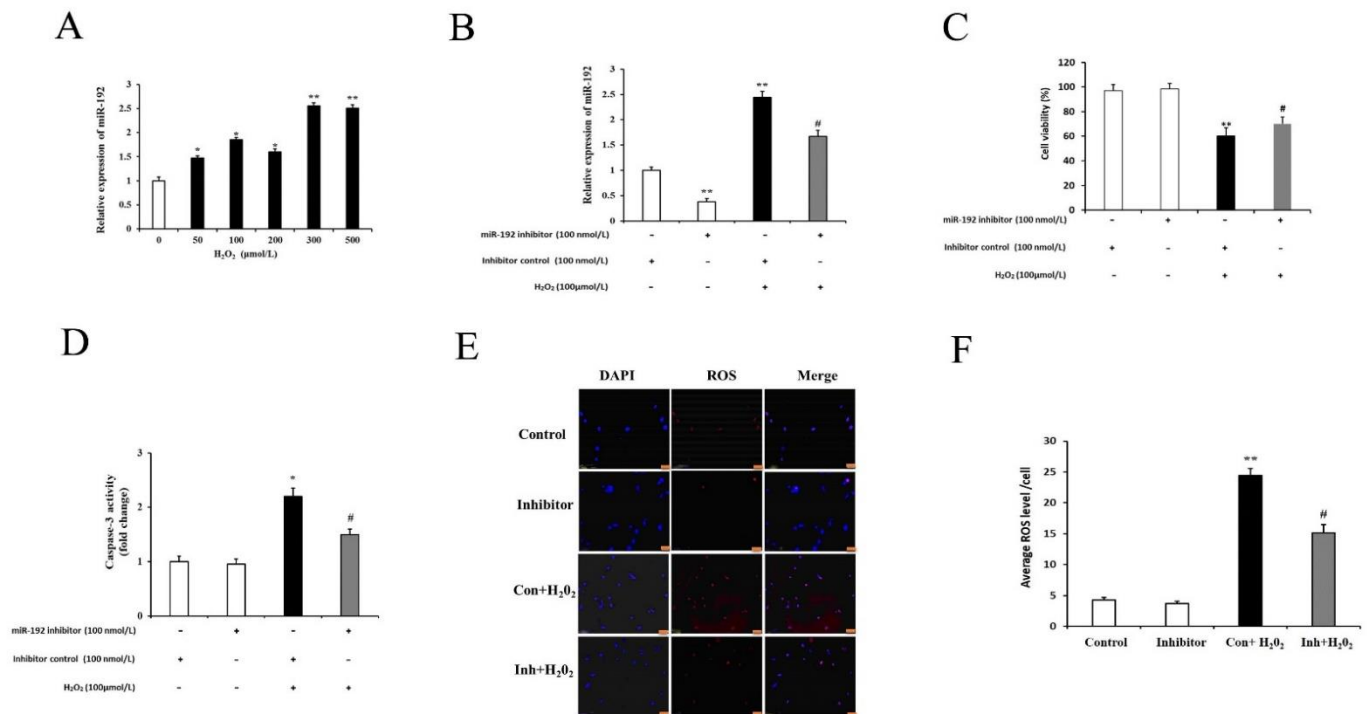


Figure 8. Downregulation of miR-192 alleviates H₂O₂-induced PGC injury. (A) The expression levels of miR192 in cultured PGCs were measured after 12 h of exposure to different H₂O₂ concentrations. (B) Transfection with miR-192 inhibitor decreased PGC miR-192 levels significantly. (C) Effects of miR-192 downregulation on PGC proliferation. (D) Effects of miR-192 downregulation on caspase-3 activity. (E) Effects of miR-192 downregulation on intracellular ROS levels, scale bars correspond to 50 μm. (F) Quantification of intracellular ROS levels. Each value is expressed as the mean ± S.E. ($n = 3$). * $p < 0.05$ and ** $p < 0.001$ vs. con; # $p < 0.01$ Inh + H₂O₂ vs. con+ H₂O₂.

3.7. miR 192a Knockdown Inhibits PGC Oxidative Damage through the Upregulation of *Acvr2a* and Suppression of Caspase-3 Activity

ACVR2A expression regulation was previously found to be closely associated with GC proliferation [23]. Therefore, we further studied whether miR-192 knockdown may exert a protective effect against H₂O₂-induced PGC apoptosis. As shown in Figure 10A,B, the expression levels of *Acvr2a* mRNA and the ACVR2A protein were significantly downregulated in the inhibitor control plus H₂O₂-treated PGCs compared with H₂O₂-free PGCs, and this decreased expression could be significantly increased by miR-192 knockdown. In contrast, PGCs transfected with the miR-192 inhibitor increased their expression levels of *Acvr2a* mRNA and the ACVR2A protein in the H₂O₂-induced PGCs. Furthermore, the caspase-3 mRNA expression and cleaved caspase-3 protein level were increased in the inhibitor control plus H₂O₂-treated PGCs compared with H₂O₂-free PGCs; this increased expression was reduced by miR-192 knockdown ($p < 0.05$; Figure 10C,D). These results suggest that miR-192 promotes H₂O₂-induced PGC apoptosis by modulating the expression of *Acvr2a* and caspase-3.

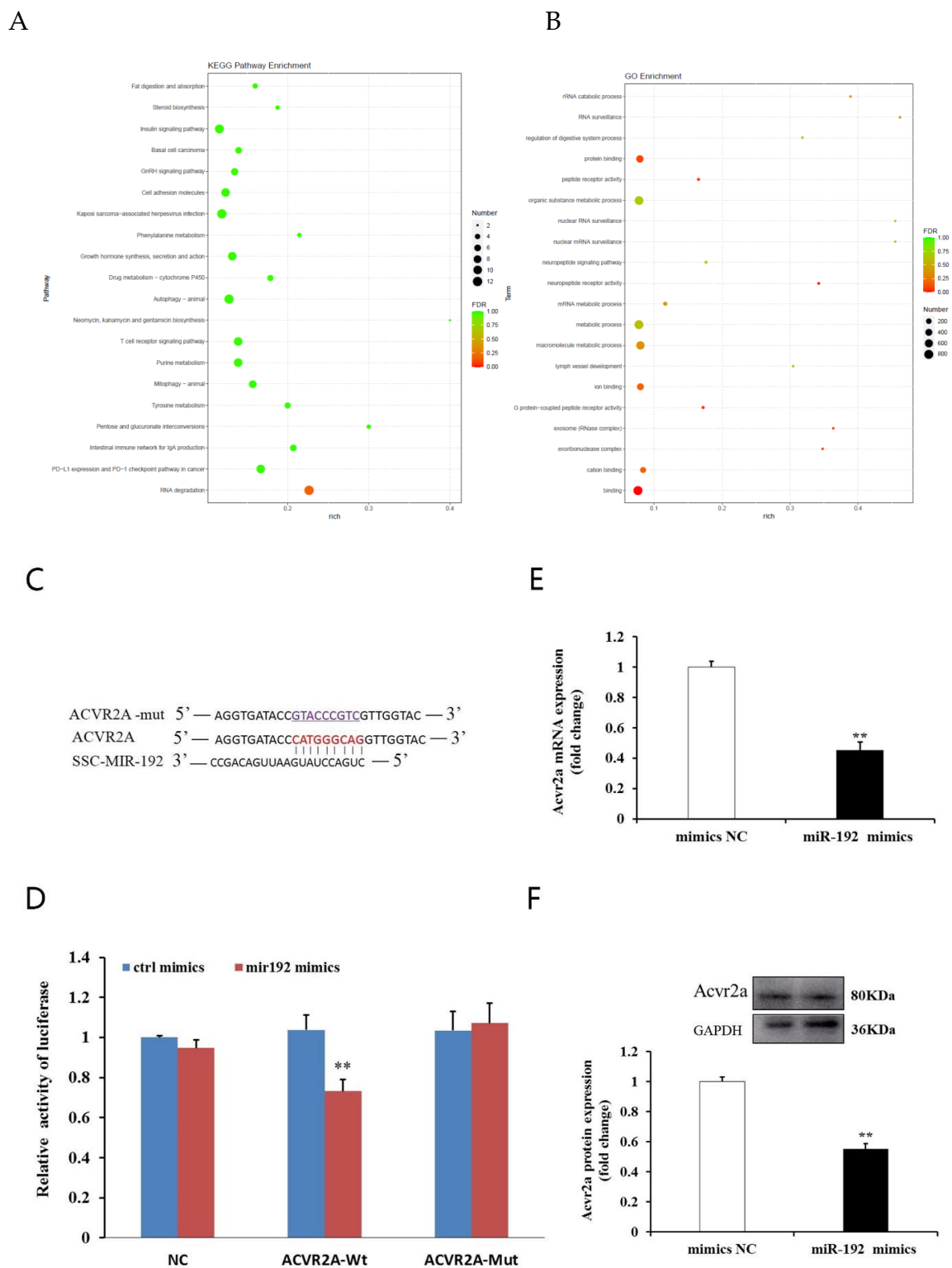


Figure 9. Identification of the miR-192 target gene. (A) Bubble chart indicating the KEGG pathways associated with miR-192 targets. (B) GO enrichment analysis of miR-192 targets. (C) The predicted binding region between miR-192 and Acvr2a mRNA was predicted using bioinformatics analysis. (D) Luciferase activity assay. (E) The mRNA expression of Acvr2a was assessed in GCs transfected with miR-192 mimics via RT-PCR. (F) At 48 h post-transfection, ACVR2A protein level in cultural PGCs was determined via Western blotting. GAPDH expression levels were used to normalize protein levels. Data are presented as means ± SE. (n = 3). ** p < 0.01.

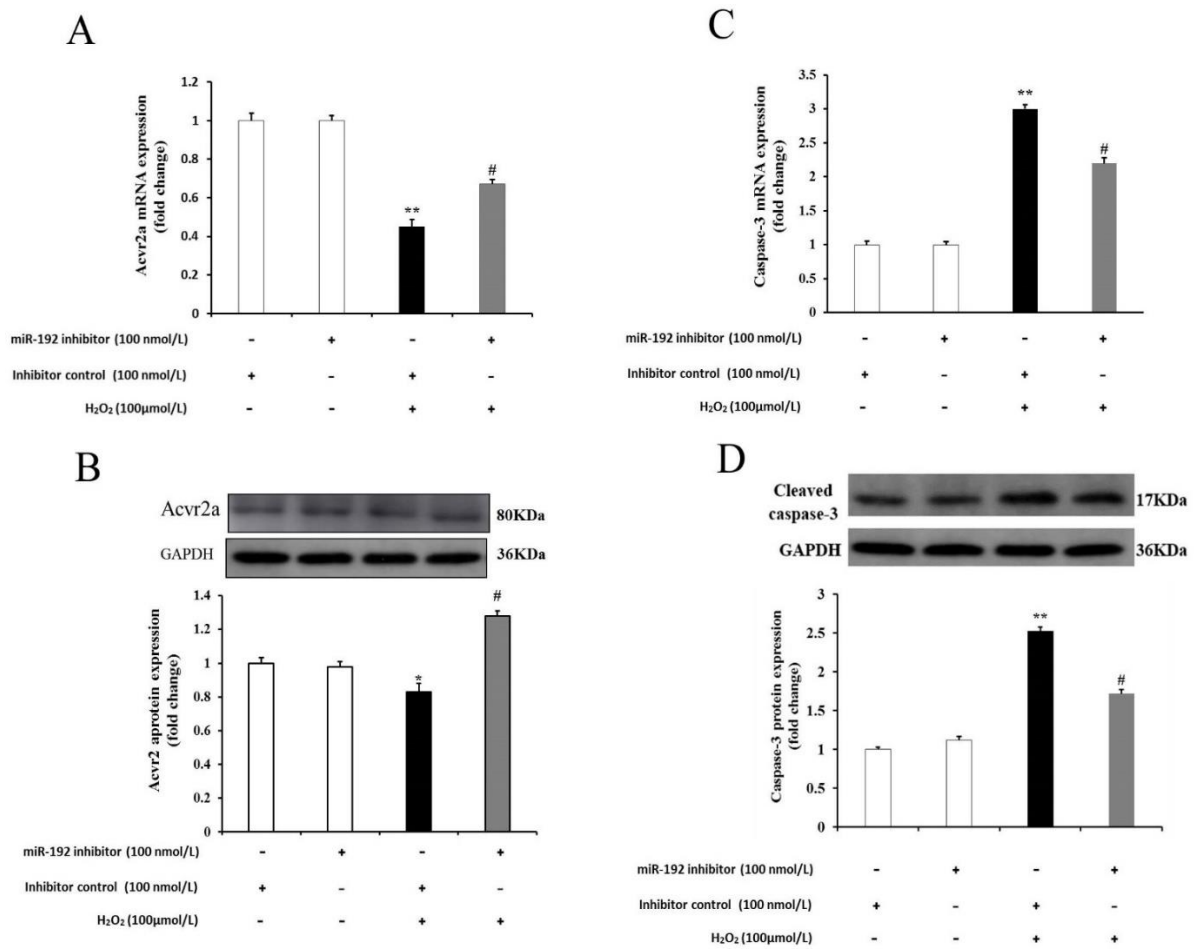


Figure 10. Downregulation of miR-192 attenuates H₂O₂-induced oxidative injury in PGCs through the regulation of Acvr2a and caspase-3. (A) Effects of miR-192 downregulation on the mRNA expression of Acvr2a. (B) Effects of miR-192 downregulation on the protein expression of ACVR2A. (C) Effects of miR-192 downregulation on the mRNA expression of caspase-3. (D) Effects of miR-192 downregulation on the protein levels of cleaved caspase-3. Data are shown as mean ± SE. (n = 3). * p < 0.05, ** p < 0.01 vs. the H₂O₂-free group (control); # p < 0.05 vs. the H₂O₂ plus inhibitor control.

3.8. Acvr2a Is Required for GSPB2-Mediated PGC Protection against Oxidative Damage

Grape seed procyanidin B2 (GSPB2), a polyphenolic component found in red wine and grapes, has been reported to protect against ovarian oxidative damage [5]. To determine whether GSPB2 regulates cell viability in cultured PGCs under oxidative stress, a CCK-8 assay was employed to determine PGC viability. As shown in Figure 11A,B, H₂O₂ significantly reduced PGC viability in a dose-dependent manner, and PGCs pretreated with GSPB2 displayed a marked increase in GSPB2-plus-H₂O₂-treated PGCs compared with H₂O₂-treated PGCs. The inhibition of Acvr2a expression has been suggested to inhibit GC proliferation and induce apoptosis [23]. To explore whether Acvr2a correlates with GSPB2-mediated apoptosis inhibition during oxidative stress, the transcript encoding Acvr2a was inhibited using RNA interference. As shown in Figure 11C, the expression level of Acvr2a mRNA was markedly lower in PGCs transfected with siRNA plus H₂O₂ than those transfected with the SC siRNA. PGCs pretreated with GSPB2 significantly increased the expression level of Acvr2a mRNA. Furthermore, Acvr2a knockdown significantly inhibited the viability of PGCs compared with those transfected with the SC siRNA. PGCs pretreated with GSPB2 exhibited an increase in viability compared with untreated control cells Figure 11D. In addition, by measuring caspase-3 activity under the same conditions

(Figure 11E), we further confirmed that Acvr2a is required for GSPB2-mediated PGC protection against oxidative injury.

3.9. GSPB2 Protects PGCs from H₂O₂-Induced Oxidative Damage through the Downregulation of miR-192

Previous studies have revealed that GSPB2 exhibits inhibitory effects on GC oxidative damage [24]. To determine whether GSPB2 supplement affects the expression of endogenous miR-192 in PGCs, the PGCs were pretreated with GSPB2 for 12 h and, finally, incubated with H₂O₂ for 12 h, and the expression of miR-192 was determined via qRT-PCR. As shown in Figure 12A, PGCs treated with H₂O₂ significantly enhanced the expression of miR-192 compared with control group, and GSPB2 supplement significantly suppressed the H₂O₂-induced upregulation of miR-192 expression in PGCs ($p < 0.05$). Cell viability assays showed that the transfection of the miR-192 inhibitor resulted in the upregulation of PGC viability induced by H₂O₂, and the transfection of the miR-192 mimics resulted in the downregulation of PGC viability induced by H₂O₂ ($p < 0.05$) (Figure 12B,D). Furthermore, the caspase-3 activity assays indicated that transfection of the miR-192 inhibitor caused the downregulation of caspase-3 activity in H₂O₂-treated PGCs ($p < 0.05$). In contrast, PGCs transfected with miR-192 mimics resulted in the upregulation of caspase-3 activity in H₂O₂-treated PGCs ($p < 0.05$) (Figure 12C,E). These results indicate that GSPB2 suppressed H₂O₂-induced PGC oxidative injury by regulating miR-192 expression.

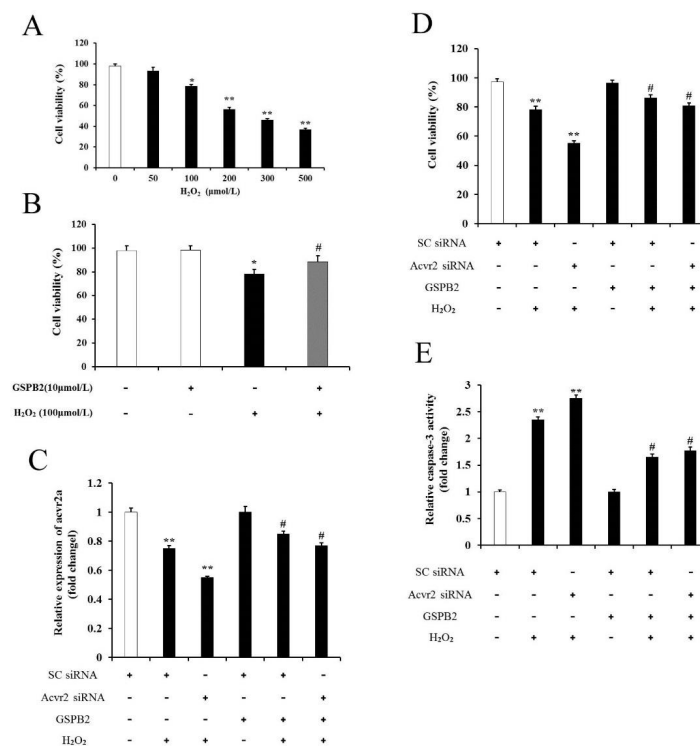


Figure 11. Acvr2a involved in GSPB2-mediated PGC protection during oxidative stress. (A) Primary cultured PGCs were treated with different concentrations of H₂O₂ for 12 h. Cell viability was then determined using CCK-8 assay. (B) PGCs were pretreated with or without GSPB2 (10 μM) for 12 h, rinsed in PBS, and then, incubated with 100 μM H₂O₂ for 12 h. Cells were then collected for measurement of cell viability. * $p < 0.05$, ** $p < 0.01$ vs. control group; # $p < 0.05$ vs. the H₂O₂-treated group. Data are shown as mean ± SE ($n = 3$). (C) PGCs transfected with Acvr2a siRNA or scrambled control siRNA for 24 h were cultured for another 12 h in the presence or absence of 10 μM GSPB2, and then, incubated with 100 μM H₂O₂ for 12 h. The mRNA expression of Acvr2a was determined via qRT-PCR. (D) Cell viability was determined using the CCK-8 assay. (E) Caspase-3 activity was measured using ELISA. Data are shown as mean ± SE. ($n = 3$). ** $p < 0.05$ vs. SC siRNA-alone group; # $p < 0.05$ vs. SC siRNA plus GSPB2 pretreatment.

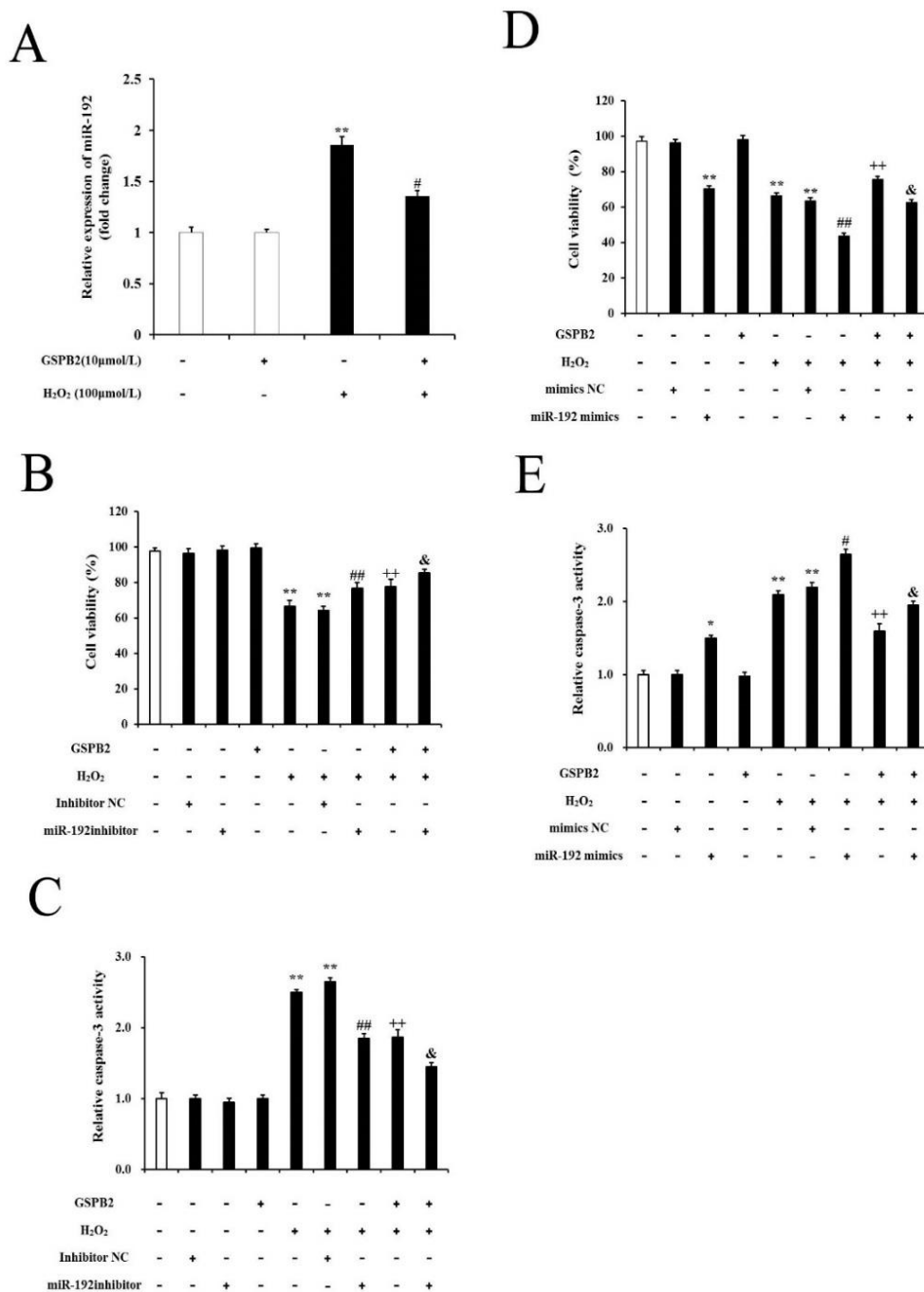


Figure 12. GSPB2 counteracts H₂O₂-induced PGC injury through the regulation of miR-192. (A) PGCs were pretreated with or without GSPB2 (10 μM) for 12 h, rinsed in PBS, and then, incubated with 100 μM H₂O₂ for 12 h. The expression of miR-192 was determined via qRT-PCR. Data are shown as mean ± SE. (n = 3). ** p < 0.01 vs. the control; ## p < 0.05 vs. H₂O₂ group. (B) PGCs were transfected with miR-192 inhibitor for 24 h; then, they were treated with or without GSPB2 (10 μM) for 12 h, and finally, incubated with H₂O₂ (100 μM) for 12 h. A CCK-8 assay was used to determine PGC viability. (C) PGCs were treated as above. The detection of caspase-3 activity was conducted via ELISA assay. (D) PGCs were transfected with miR-192 mimic for 24 h; then, they were treated with or without GSPB2 (10 μM) for 12 h, and finally, incubated with H₂O₂ (100 μM) for 12 h. PGC viability was determined via CCK-8 assay. (E) PGCs were treated as above. Caspase-3 activity was measured via ELISA assay. Data are shown as mean ± SE. (n = 3). ** p < 0.01 vs. the control; ## p < 0.01 vs. H₂O₂ plus miR-192 inhibitor; ++ p < 0.01 vs. GSPB2-alone group; & p < 0.05 vs. the GSPB2-plus-H₂O₂ group. * p < 0.05, # p < 0.05.

4. Discussion

The ovarian follicle is a primary site for the production of steroid hormones and is vital for normal ovarian function and female reproduction. Although the mammalian ovaries contain numerous preantral follicles at different stages, more than 99% of the follicles are destroyed through follicular atresia, which has been found to be the primary cause of GC apoptosis. OS, which is caused by the overproduction of ROSs and an impaired antioxidant defense system, is also involved in GC apoptosis. Several factors, such as injury, inflammation, smoking, nutrient loss, and aging, are known to accelerate GC apoptosis, resulting in follicular atresia [8]. On the contrary, OS inhibitors suppress GC apoptosis during follicular atresia. For example, OS-induced apoptosis in preovulatory follicles was blocked by treatment with FSH and was related to enhanced GSH synthesis [25]. Proanthocyanidins may protect humans and PGCs against OS-induced apoptosis [24,26]. As master regulators of gene expression, miRNAs may play a significant role in OS-induced GC death. Here, we found that H₂O₂ (100 μM and 300 μM) could induce ROS generation, promote cell apoptosis, and decrease cell viability in vitro.

miRNAs function as post-transcriptional gene-expression regulators by inhibiting protein translation or by targeting mRNAs for degradation. Accumulating evidence has shown that OS significantly alters miRNA expression in several cell types, including human, mouse, and bovine cells [27–29]. Furthermore, miRNAs have been shown to be the major regulators under conditions of OS [30]. Importantly, studies have substantiated the role of miRNAs in almost all adverse events occurring in the female reproductive system, including PCOS, POE, and POI. It has also been shown that a number of miRNAs may be involved in regulating GC proliferation (i.e., miR-145 and miR-224), differentiation (i.e., miR-224, miR-383, and miR-378), and apoptosis (i.e., miR-23a, miR-21, and miR-26b) [6,31]. In this study, we identified 22 DEmiRNAs (14 upregulated and 8 downregulated) in the LOS group and 33 DEmiRNAs (19 upregulated and 14 downregulated) in the MON group through miRNA-Seq ($|\log_2(\text{fold change})| \geq 1$ and $p\text{-value} < 0.05$). Moreover, several of these miRNAs have been proven to be regulated by various stimuli in different types of cells. For example, a higher expression of miR-200c triggered by OS in vitro significantly attenuates cell growth and induces apoptosis and senescence in human umbilical vein endothelial cells [32]. miR-27a-5p has been proven to be induced by inflammatory stimuli, such as Ox-PAPC, IL-1β and TNFα, which subsequently modulate the extent of NF-κB signaling in HUVECs [33]. The miR-375 levels were significantly upregulated in doxorubicin-treated rat and mouse cardiomyocytes, and the inhibition of miR-375 reduced inflammation and increased the survival of cardiomyocytes [34]. Additionally, several DEmiRNAs, such as miR-139-3p, miR-190b, and miR-19b, are known to be involved in proliferation, growth, aging and apoptosis in HeLa cells, follicular fluid, and SH-SY5Y cells by targeting NOB1, EXT1, and HAPLN4, respectively [35–37].

Additionally, OS may trigger or mediate multiple signaling pathways to regulate cellular processes, such as the PI3K-Akt [38], FoxO [10], mTOR [39], NF-κB [40], and JNK signaling pathways [41]. Here, we identified the top 20 pathways in PGCs following exposure to OS through the enrichment analysis of multiple miRNA target genes (Figure 3B,D). Interestingly, we observed that the signaling pathways mentioned above also existed in our enrichment analysis. Furthermore, Ras signaling, Rap1 signaling, and pathways in cancer were also enriched. Several of these pathways play a role in cell survival, autophagy, and apoptosis. For example, the FoxO and NF-κB signaling pathways are directly involved in the survival of porcine and mouse GCs [38,39,42,43]. Moreover, PI3K-Akt activation and JNK inhibition have been shown to inhibit apoptosis in porcine and mouse GCs in response to OS [38,42,44]. Pathway analysis of our data suggests that OS might induce the initiation and development of PGC death by inhibiting the activation of pathways related to cell survival and activating proapoptotic pathways.

Previous studies have demonstrated that OS significantly alters gene expression in different types of cells [10,26,32]. Here, a network, consisting of target mRNAs and dysregulated miRNAs obtained from the LOS group and MON group versus CON, was

constructed (Figure 5). Moreover, multiple hub genes, including FoxO1, TGFBR1, ACVR1B, SMAD3, SMAD7, BMPR2, XIAP, and ESR1, were identified. Among them, FoxO1, a key modulator of stress, has been proven to be regulated by H₂O₂-induced OS at different levels [6,10]. SMAD3, BMPR2, XIAP, and ESR1 have also been proven to be regulated by OS in skin fibroblasts [45], vascular smooth-muscle cells [46], PC6.3 cells [47], and breast cancer [48]. In addition, these genes have been reported to be major regulators affecting cell state and function. For instance, TGFB1, BMP7, BMP6, BMPR2, SMAD3, SMAD1, and SMAD7 are involved in cell proliferation and apoptosis. ACVR1B, ESR1, TGFBR1, and NR5A1 are associated with hormone secretion and cytokine responses. FoxO1, XIAP, BAD, ATG12, FAS, and GADD45B are apoptosis and autophagy factors. The functions of these miRNA target genes could partially explain the effects of H₂O₂-induced OS on PGC function and state.

miRNAs are known to play essential roles in several cellular processes [49,50]. In this study, we performed miRNA–GO network analysis based on the relationship between significant biological functions and miRNAs. The results showed that MAPK activity, the apoptotic process, the cellular response to DNA damage stimulus, the TGF- β receptor signaling pathway, and positive regulation of the proliferation of the cellular population were enriched in the miRNA–GO regulatory network. Moreover, these biological processes were associated with different cell types. For example, it was found that the miR-19b-induced anti-apoptosis effect was promoted by the MAPK pathway in SH-SY5Y cells [37]. miR139-3p may act as a tumor suppressor that inhibits cell migration, proliferation, and invasion, and induces cell apoptosis through the downregulation of NOB1 expression [35]. In addition, miR-192 can target the RB1 gene to induce lung cancer cell apoptosis through the caspase pathway [51]. Thus, these data indicate that H₂O₂-induced OS may regulate the biological functions of PGCs by altering the expression of specific miRNAs.

Recent studies suggest that miR-192 is regulated by hypoxia and oxidative stress. For instance, in the ovary of the marine medaka, miR-192 was found to be statistically significantly upregulated under hypoxia [21], suggesting that miR-192 plays a regulatory role in ovaries under hypoxic stress. In endothelial cells (ECs), Paola et al. reported that miR-192 was most induced by oxidative stress, and miR-192 overexpression significantly decreased ECs proliferation and induced EC death, indicating that miR-192 has a potential role in cell survival [20]. The results of this study show that miR-192 levels are significantly increased in the PGCs subjected to H₂O₂ exposure. MiR-192 knockdown enhances cell viability and reduces caspase-3 activity following H₂O₂ incubation (Figure 8). ACVR2A is a critical regulator of follicle development in mammals [52]. Acvr2a knockdown can lead to the inhibition of GC proliferation [23]. Our current study indicates that miR-192 overexpression reduces Acvr2a mRNA and ACVR2A protein levels in PGCs by targeting Acvr2a 3'UTR (Figure 9). Furthermore, the mRNA and protein expression levels of Acvr2a decrease in PGCs after H₂O₂ exposure, and miR-192 knockdown significantly enhances Acvr2a levels. These findings indicate that increases in miR-192 expression and decreases in Acvr2a expression resulting from H₂O₂ treatment cause PGC oxidative injury.

Our findings show that miR-192 expression is significantly upregulated in PGCs following H₂O₂ treatment. This finding is in line with those of previous reports [20,21]. Furthermore, miR-192 expression is markedly increased in GCs of women's with diminished ovarian reserves [53], suggesting that it might be connected to GC proliferation and survival. Therefore, we further studied the role of miR-192 in H₂O₂-triggered PGC damage. Using overexpression, knockdown, bioinformatic analysis, luciferase assays, and mRNA and protein expression analyses, we confirmed that Acvr2a is a target of miR-192. Acvr2a is the critical receptor type II A of activin, a member of the transforming growth factor-beta (TGF- β) superfamily through which activin or related TGF- β ligands induce FSH production [54]. In mice, the inhibition of Acvr2a expression results in GC apoptosis [23]. Furthermore, targeted depletion of Acvr2a in mice increased the number of atretic follicles [55]. The results herein show that Acvr2a expression is markedly decreased in H₂O₂-treated GC apoptosis. Furthermore, miR-192 inhibition markedly reverses the expression of Acvr2a

mRNA and the ACVR2A protein during H₂O₂ exposure (Figure 10). These results indicate that Acvr2a is a direct target of miR-192 and that it mediates the role of miR-192 in PGC oxidative damage during H₂O₂ exposure. Meanwhile, all of these findings lead us to speculate that miR-192 mediates H₂O₂-induced PGC apoptosis by suppressing Acvr2a expression, resulting in the dephosphorylation of type I receptors and the inactivation of intracellular R-Smad signal transducers, thereby increasing the relative abundance of Bim and Bax and causing caspase-3-mediated apoptosis.

GSPB2 is one of the main components of grape seed proanthocyanidin extract (GSPE). Growing evidence suggest that GSPB2 alleviates oxidative-stress-activated GC apoptosis [24,26]. In this study, we found that PGCs pretreated with GSPB2 for 12 h dramatically inhibit the cell-viability loss triggered by H₂O₂. Furthermore, GSPB2 markedly inhibited caspase-3 activity induced by H₂O₂ in PGCs, which was associated with the increasing expression of Acvr2a (Figure 11). Here, we aimed to elucidate the key role of miR-192 in PGC injury triggered by H₂O₂, and whether GSPB2-mediated PGC protection is correlated with miR-192 regulation. Our data suggest that the expression level of miR-192 is markedly increased in PCs treated with H₂O₂, but this level is significantly decreased in PGCs pretreated with GSPB2 prior to H₂O₂. Moreover, miR-192 knockdown enhanced the cytoprotective role of GSPB2 against H₂O₂-triggered PGC damage. Collectively, these data demonstrate that the cytoprotective role of GSPB2 against H₂O₂-triggered PGC damage occurs partially through the downregulation of miR-192.

5. Conclusions

In conclusion, the depression of miR-192 alleviates oxidative stress by directly targeting Acvr2a in H₂O₂-caused PGC damage. miR-192/Acvr2a might act as a potential and novel therapeutic target for oxidative-stress-induced PGC injury. These results also provide important insights into the potential discovery and development of GSPB2 as a novel drug for reproductive-disease treatment.

Supplementary Materials: The following supporting information can be downloaded at: <https://www.mdpi.com/article/10.3390/cells11152362/s1>, Supplementary Table S1: up- and downregulated miRNAs in H₂O₂-treated porcine GCs; Supplementary Table S2: predicted target genes of differentially expressed miRNAs in 100 μM H₂O₂-treated porcine GCs; Supplementary Table S3: predicted target genes of differentially expressed miRNAs in 300 μM H₂O₂-treated porcine GCs. Supplementary Table S4: pathways regulated by 13 differentially expressed miRNAs; Supplementary Table S5: genes regulated by 13 differentially expressed miRNAs; Supplementary Table S6: biological processes regulated by 13 differentially expressed miRNAs.

Author Contributions: Conceptualization, J.Z. and B.X.; writing—original draft preparation, J.Z., J.C., J.W., X.W. and B.X.; writing—review and editing, J.Z., Q.R., L.L. and M.S. All authors have read and agreed to the published version of the manuscript.

Funding: This research supported by the Natural Science Foundation of Henan Province (202300410529), the Fund for Distinguished Young Scholars from the Henan Academy of Agricultural Sciences (2021JQ07), and the Science and Technology Project of Henan Province (222102110096, 222102110467).

Institutional Review Board Statement: The study was conducted in accordance with the guidelines of the Institutional Animal Care and Use Committee of Animal Husbandry and Veterinary Science, Henan Academy of Agricultural Sciences. The approval number for this study is IACUC-20190820002.

Informed Consent Statement: Not applicable.

Data Availability Statement: The sequence data from this study have been submitted to the NCBI Gene Expression Omnibus (GEO) under the accession number GSE201369.

Conflicts of Interest: The authors declare no conflict of interest.

References

1. Zhang, J.-Q.; Gao, B.-W.; Guo, H.-X.; Ren, Q.-L.; Wang, X.-W.; Chen, J.-F.; Wang, J.; Zhang, Z.-J.; Ma, Q.; Xing, B.-S. miR-181a promotes porcine granulosa cell apoptosis by targeting TGFBR1 via the activin signaling pathway. *Mol. Cell. Endocrinol.* **2019**, *499*, 110603. [[CrossRef](#)] [[PubMed](#)]
2. Tu, J.; Cheung, H.H.; Chan, C.L.-K.; Chan, W.Y. The Role of microRNAs in Ovarian Granulosa Cells in Health and Disease. *Front. Endocrinol.* **2019**, *10*, 174. [[CrossRef](#)] [[PubMed](#)]
3. Saller, S.; Kunz, L.; Berg, D.; Berg, U.; Lara, H.; Urrea, J.; Hecht, S.; Pavlik, R.; Thaler, C.; Mayerhofer, A. Dopamine in human follicular fluid is associated with cellular uptake and metabolism-dependent generation of reactive oxygen species in granulosa cells: Implications for physiology and pathology. *Hum. Reprod.* **2014**, *29*, 555–567. [[CrossRef](#)] [[PubMed](#)]
4. Giuseppina, B.; Bussolati, S.; Sujen Eleonora, S.; Francesca, G. Reactive oxygen species and anti-oxidant defences in swine follicular fluids. *Reprod. Fertil. Dev.* **2008**, *20*, 269.
5. Zhang, J.-Q.; Gao, B.-W.; Wang, J.; Ren, Q.-L.; Chen, J.-F.; Ma, Q.; Zhang, Z.-J.; Xing, B.-S. Critical Role of FoxO1 in Granulosa Cell Apoptosis Caused by Oxidative Stress and Protective Effects of Grape Seed Procyanidin B2. *Oxidative Med. Cell. Longev.* **2016**, *2016*, 6147345. [[CrossRef](#)]
6. Zhang, M.; Zhang, Q.; Hu, Y.; Xu, L.; Jiang, Y.; Zhang, C.; Ding, L.; Jiang, R.; Sun, J.; Sun, H.; et al. miR-181a increases FoxO1 acetylation and promotes granulosa cell apoptosis via SIRT1 downregulation. *Cell Death Dis.* **2017**, *8*, e3088. [[CrossRef](#)]
7. Luderer, U. Ovarian Toxicity from Reactive Oxygen Species. *Vitam. Horm.* **2014**, *94*, 99–127. [[CrossRef](#)]
8. Devine, P.J.; Perreault, S.D.; Luderer, U. Roles of Reactive Oxygen Species and Antioxidants in Ovarian Toxicity1. *Biol. Reprod.* **2012**, *86*, 27. [[CrossRef](#)]
9. Jia-Qing, Z.; Ming, S.; Cheng-Cheng, Z.; Feng-Xiang, Y.; Ze-Qun, L.; Nazim, A.; Shao-Chen, S.; Kui, L.; Hong-Lin, L. 3-nitropropionic acid induces ovarian oxidative stress and impairs follicle in mouse. *PLoS ONE* **2014**, *9*, e86589.
10. Ming, S.; Fei, L.; Jiaqing, Z.; Yiting, T.; Wei-Kang, C.; Honglin, L. Involvement of the up-regulated foxo1 expression in follicular granulosa cell apoptosis induced by oxidative stress. *J. Biol. Chem.* **2012**, *287*, 25727–25740.
11. Roy, C.; Lavoie, M.; Richard, G.; Archambault, A.; Lapointe, J. Evidence that oxidative stress is higher in replacement gilts than in multiparous sows. *J. Anim. Physiol. Anim. Nutr.* **2016**, *100*, 911–919. [[CrossRef](#)]
12. Yang, Y.Y.; Hu, C.J.; Zhao, X.C.; Xiao, K.L.; Deng, M.; Zhang, L.; Qiu, X.G.; Deng, J.P.; Yin, Y.L.; Tan, C.Q. Dietary energy sources during late gestation and lactation of sows: Effects on performance, glucolipid metabolism, oxidative status of sows, and their offspring1. *J. Anim. Sci.* **2019**, *97*, 4608–4618. [[CrossRef](#)] [[PubMed](#)]
13. Zhang, J.; Xu, Y.; Liu, H.; Pan, Z. Micrnas in ovarian follicular atresia and granulosa cell apoptosis. *Reprod. Biol. Endocrinol.* **2019**, *17*, 9. [[CrossRef](#)] [[PubMed](#)]
14. Donadeu, F.X.; Schauer, S.N.; Sontakke, S.D. Involvement of miRNAs in ovarian follicular and luteal development. *J. Endocrinol.* **2012**, *215*, 323–334. [[CrossRef](#)]
15. Xu, L.; Sun, H.; Zhang, M.; Jiang, Y.; Zhang, C.; Zhou, J.; Ding, L.; Hu, Y.; Yan, G. MicroRNA-145 protects follicular granulosa cells against oxidative stress-induced apoptosis by targeting Krüppel-like factor 4. *Mol. Cell. Endocrinol.* **2017**, *452*, 138–147. [[CrossRef](#)]
16. Cao, R.; Wu, W.; Zhou, X.; Liu, K.; Li, B.; Huang, X.; Zhang, Y.; Liu, H. Let-7g induces granulosa cell apoptosis by targeting MAP3K1 in the porcine ovary. *Int. J. Biochem. Cell Biol.* **2015**, *68*, 148–157. [[CrossRef](#)] [[PubMed](#)]
17. Lee, B.M.; Chun, J.L.; Lee, J.H.; Kim, E.Y.; Park, K.-S.; Lee, J.-H.; Daigneault, B.W.; Smith, G.W.; Kim, K.J.; Chang, K.-T.; et al. Follistatin Rescues Blastocyst Development of Poor Quality Porcine Cumulus-Oocyte Complexes by Delaying Meiotic Resumption with Decreased cGMP. *Reprod. Sci.* **2018**, *25*, 759–772. [[CrossRef](#)]
18. Wei, H.-K.; Zhou, Y.; Jiang, S.; Tao, Y.-X.; Sun, H.; Peng, J.; Jiang, S. Feeding a DHA-enriched diet increases skeletal muscle protein synthesis in growing pigs: Association with increased skeletal muscle insulin action and local mRNA expression of insulin-like growth factor 1. *Br. J. Nutr.* **2013**, *110*, 671–680. [[CrossRef](#)] [[PubMed](#)]
19. Livak, K.J.; Schmittgen, T.D. Analysis of relative gene expression data using real-time quantitative pcr and the 2(-delta delta c(t)) method. *Methods* **2001**, *25*, 402–408. [[CrossRef](#)]
20. Fuschi, P.; Carrara, M.; Voellenkle, C.; Garcia-Manteiga, J.M.; Righini, P.; Maimone, B.; Sangalli, E.; Villa, F.; Specchia, C.; Picozza, M.; et al. Central role of the p53 pathway in the noncoding-RNA response to oxidative stress. *Aging* **2017**, *9*, 2559–2586. [[CrossRef](#)]
21. Lai, K.P.; Li, J.-W.; Tse, A.C.-K.; Chan, T.-F.; Wu, R.S.-S. Hypoxia alters steroidogenesis in female marine medaka through miRNAs regulation. *Aquat. Toxicol.* **2016**, *172*, 1–8. [[CrossRef](#)] [[PubMed](#)]
22. Dong, L.; Vaux, D.L. Glucocorticoids can induce BIM to trigger apoptosis in the absence of BAX and BAK1. *Cell Death Dis.* **2020**, *11*, 442. [[CrossRef](#)] [[PubMed](#)]
23. Zhang, Q.; Sun, H.; Jiang, Y.; Ding, L.; Wu, S.; Fang, T.; Yan, G.; Hu, Y. MicroRNA-181a Suppresses Mouse Granulosa Cell Proliferation by Targeting Activin Receptor IIA. *PLoS ONE* **2013**, *8*, e59667. [[CrossRef](#)] [[PubMed](#)]
24. Barbe, A.; Ramé, C.; Mellouk, N.; Estienne, A.; Bongrani, A.; Brossaud, A.; Riva, A.; Guérif, F.; Froment, P.; Dupont, J. Effects of Grape Seed Extract and Proanthocyanidin B2 on In Vitro Proliferation, Viability, Steroidogenesis, Oxidative Stress, and Cell Signaling in Human Granulosa Cells. *Int. J. Mol. Sci.* **2019**, *20*, 4215. [[CrossRef](#)]
25. Miyun, T.T.; Ulrike, L. Opposing effects of glutathione depletion and follicle-stimulating hormone on reactive oxygen species and apoptosis in cultured preovulatory rat follicles. *Endocrinology* **2006**, *147*, 1224–1236.

26. Zhang, J.-Q.; Wang, X.-W.; Chen, J.-F.; Ren, Q.-L.; Wang, J.; Gao, B.-W.; Shi, Z.-H.; Zhang, Z.-J.; Bai, X.-X.; Xing, B.-S. Grape Seed Procyandin B2 Protects Porcine Ovarian Granulosa Cells against Oxidative Stress-Induced Apoptosis by Upregulating let-7a Expression. *Oxidative Med. Cell. Longev.* **2019**, *2019*, 1076512. [[CrossRef](#)]
27. Luo, Y.; Wen, X.; Wang, L.; Gao, J.; Wang, Z.; Zhang, C.; Zhang, P.; Lu, C.; Duan, L.; Tian, Y. Identification of MicroRNAs Involved in Growth Arrest and Apoptosis in Hydrogen Peroxide-Treated Human Hepatocellular Carcinoma Cell Line HepG2. *Oxidative Med. Cell. Longev.* **2016**, *2016*, 7530853. [[CrossRef](#)]
28. Fatemi, N.; Sanati, M.H.; Shamsara, M.; Moayer, F.; Zavarehei, M.J.; Pouya, A.; Sayyehpour, F.; Ayat, H.; Gourabi, H. TBHP-induced oxidative stress alters microRNAs expression in mouse testis. *J. Assist. Reprod. Genet.* **2014**, *31*, 1287–1293. [[CrossRef](#)]
29. Soheli, M.H.; Akyuz, B.; Konca, Y.; Arslan, K.; Sariozkan, S.; Cinar, M.U. Oxidative stress modulates the expression of apoptosis-associated microRNAs in bovine granulosa cells in vitro. *Cell Tissue Res.* **2019**, *376*, 295–308. [[CrossRef](#)]
30. Ebrahimi, S.O.; Reisi, S.; Shareef, S. miRNAs, oxidative stress, and cancer: A comprehensive and updated review. *J. Cell. Physiol.* **2020**, *235*, 8812–8825. [[CrossRef](#)]
31. Chunxue, Z.; Jingtao, S.; Shuangbo, K.; Mei, Z.; Qun, Z.; Jidong, Z.; Xin, Z.; Nannan, K.; Yue, J.; Lijun, D. MicroRNA-181a promotes follicular granulosa cell apoptosis via sphingosine-1-phosphate receptor 1 expression downregulation. *Biol. Reprod.* **2019**, *5*, 975–985.
32. Magenta, A.; Cencioni, C.; Fasanaro, P.; Zaccagnini, G.; Greco, S.; Sarra-Ferraris, G.; Capogrossi, M.C. Mir-200c is upregulated by oxidative stress and induces endothelial cell apoptosis and senescence via zeb1 inhibition. *Cell Death Differ.* **2011**, *18*, 1628–1639. [[CrossRef](#)] [[PubMed](#)]
33. Romay, M.C.; Che, N.; Becker, S.N.; Pouldar, D.; Hagopian, R.; Xiao, X.; Lusic, A.J.; Berliner, J.A.; Civelek, M. Regulation of nf-kb signaling by oxidized glycerophospholipid and il-1 β induced mirs-21-3p and -27a-5p in human aortic endothelial cells. *J. Lipid Res.* **2015**, *56*, 38–50. [[CrossRef](#)]
34. Zhang, H.; Tian, Y.; Liang, D.; Fu, Q.; Jia, L.; Wu, D.; Zhu, X. The Effects of Inhibition of MicroRNA-375 in a Mouse Model of Doxorubicin-Induced Cardiac Toxicity. *Med. Sci. Monit.* **2020**, *26*, e920557-1–e920557-13. [[CrossRef](#)] [[PubMed](#)]
35. Huang, P.; Xi, J.; Liu, S. MiR-139-3p induces cell apoptosis and inhibits metastasis of cervical cancer by targeting NOB1. *Biomed. Pharmacother.* **2016**, *83*, 850–856. [[CrossRef](#)] [[PubMed](#)]
36. Diez-Fraile, A.; Lammens, T.; Tilleman, K.; Witkowski, W.; Verhasselt, B.; Sutter, P.D.; Benoit, Y.; Espeel, M.; D’Herde, K. Age-associated differential microRNA levels in human follicular fluid reveal pathways potentially determining fertility and success of in vitro fertilization. *Hum. Fertil.* **2014**, *17*, 90–98. [[CrossRef](#)]
37. Wei, L.; Geng, L.; Yong, C. Mir-19b alleviates mpp+-induced neuronal cytotoxicity via targeting the hapln4/mapk pathway in sh-sy5y cells. *RSC Adv.* **2018**, *8*, 10706–10714.
38. Shen, M.; Liu, Z.; Li, B.; Teng, Y.; Zhang, J.; Tang, Y.; Sun, S.-C.; Liu, H. Involvement of FoxO1 in the effects of follicle-stimulating hormone on inhibition of apoptosis in mouse granulosa cells. *Cell Death Dis.* **2014**, *5*, e1475. [[CrossRef](#)]
39. Shen, M.; Jiang, Y.; Guan, Z.; Cao, Y.; Li, L.; Liu, H.; Sun, S.-C. Protective mechanism of FSH against oxidative damage in mouse ovarian granulosa cells by repressing autophagy. *Autophagy* **2017**, *13*, 1364–1385. [[CrossRef](#)]
40. Shi, J.; Sun, X.; Lin, Y.; Zou, X.; Li, Z.; Liao, Y.; Zhang, H. Endothelial cell injury and dysfunction induced by silver nanoparticles through oxidative stress via ikk/nf-kb pathways. *Biomaterials* **2014**, *35*, 6657–6666. [[CrossRef](#)]
41. Liu, S.; Shen, M.; Li, C.; Wei, Y.; Meng, X.; Li, R.; Cao, Y.; Wu, W.; Liu, H. PKC δ contributes to oxidative stress-induced apoptosis in porcine ovarian granulosa cells via activating JNK. *Theriogenology* **2019**, *131*, 89–95. [[CrossRef](#)]
42. Wang, X.-L.; Wu, Y.; Tan, L.-B.; Tian, Z.; Liu, J.-H.; Zhu, D.-S.; Zeng, S.-M. Follicle-stimulating Hormone Regulates Pro-apoptotic Protein Bcl-2-interacting Mediator of Cell Death-Extra Long (BimEL)-induced Porcine Granulosa Cell Apoptosis. *J. Biol. Chem.* **2012**, *287*, 10166–10177. [[CrossRef](#)] [[PubMed](#)]
43. Gao, H.; Lin, L.; Haq, I.U.; Zeng, S.M. Inhibition of nf-kb promotes autophagy via jnk signaling pathway in porcine granulosa cells. *Biochem. Biophys. Res. Commun.* **2016**, *473*, 311–316. [[CrossRef](#)] [[PubMed](#)]
44. Cao, Y.; Shen, M.; Jiang, Y.; Sun, S.-C.; Liu, H. Melatonin reduces oxidative damage in mouse granulosa cells via restraining JNK-dependent autophagy. *Reproduction* **2018**, *155*, 307–319. [[CrossRef](#)]
45. He, T.; Quan, T.; Voorhees, J.J.; Fisher, G.J. Oxidative stress impairs tgfbeta responsiveness by coordinate down-regulation of type ii tgfbeta receptor and smad3 in primary human skin fibroblasts. *J. Investig. Dermatol.* **2009**, *129*, S41.
46. Lane, K.L.; Talati, M.; Austin, E.; Hemnes, A.R.; Johnson, J.A.; Fessel, J.P.; Blackwell, T.; Mernaugh, R.L.; Robinson, L.; Fike, C.; et al. Oxidative Injury is a Common Consequence of BMPR2 Mutations. *Pulm. Circ.* **2011**, *1*, 72–83. [[CrossRef](#)] [[PubMed](#)]
47. Kairisalo, M.; Bonomo, A.; Hyrskyluoto, A.; Mudò, G.; Belluardo, N.; Korhonen, L.; Lindholm, D. Resveratrol reduces oxidative stress and cell death and increases mitochondrial antioxidants and XIAP in PC6.3-cells. *Neurosci. Lett.* **2011**, *488*, 263–266. [[CrossRef](#)]
48. Mobley, J.A.; Brueggemeier, R.W. Estrogen receptor-mediated regulation of oxidative stress and DNA damage in breast cancer. *Carcinogenesis* **2004**, *25*, 3–9. [[CrossRef](#)]
49. Ebert, M.S.; Sharp, P.A. Roles for MicroRNAs in Conferring Robustness to Biological Processes. *Cell* **2012**, *149*, 515–524. [[CrossRef](#)]
50. Geula, H.; Hermona, S. Cholinesterase-targeting micrnas identified in silico affect specific biological processes. *Front. Mol. Neurosci.* **2011**, *4*, 28.

51. Feng, S.; Cong, S.; Zhang, X.; Bao, X.; Wang, W.; Li, H.; Wang, Z.; Wang, G.; Xu, J.; Du, B.; et al. MicroRNA-192 targeting retinoblastoma 1 inhibits cell proliferation and induces cell apoptosis in lung cancer cells. *Nucleic Acids Res.* **2011**, *39*, 6669–6678. [[CrossRef](#)] [[PubMed](#)]
52. Schang, G.; Ongaro, L.; Schultz, H.; Wang, Y.; Zhou, X.; Brûlé, E.; Boehm, U.; Lee, S.-J.; Bernard, D.J. Murine FSH Production Depends on the Activin Type II Receptors ACVR2A and ACVR2B. *Endocrinology* **2020**, *161*, bqaa056. [[CrossRef](#)] [[PubMed](#)]
53. Woo, I.; Christenson, L.K.; Gunewardena, S.; Ingles, S.A.; Thomas, S.; Ahmady, A.; Chung, K.; Bendikson, K.; Paulson, R.; McGinnis, L.K. Micro-RNAs involved in cellular proliferation have altered expression profiles in granulosa of young women with diminished ovarian reserve. *J. Assist. Reprod. Genet.* **2018**, *35*, 1777–1786. [[CrossRef](#)] [[PubMed](#)]
54. Ongaro, L.; Zhou, X.; Cui, Y.; Boehm, U.; Bernard, D.J. Gonadotrope-specific deletion of the BMP type 2 receptor does not affect reproductive physiology in mice. *Biol. Reprod.* **2019**, *102*, 639–646. [[CrossRef](#)]
55. Matzuk, M.M.; Kumar, T.R.; Bradley, A. Different phenotypes for mice deficient in either activins or activin receptor type II. *Nature* **1995**, *374*, 356–360. [[CrossRef](#)]